



HAL
open science

Global forest carbon uptake due to nitrogen and phosphorus deposition from 1850 to 2100

Rong Wang, Daniel S Goll, Yves Balkanski, Didier Hauglustaine, Olivier Boucher, Philippe Ciais, Ivan Janssens, Josep Peñuelas, Bertrand Guenet, Jordi Sardans, et al.

► **To cite this version:**

Rong Wang, Daniel S Goll, Yves Balkanski, Didier Hauglustaine, Olivier Boucher, et al.. Global forest carbon uptake due to nitrogen and phosphorus deposition from 1850 to 2100. *Global Change Biology*, 2017, 23 (11), pp.4854-4872. 10.1111/gcb.13766 . hal-02872389

HAL Id: hal-02872389

<https://hal.science/hal-02872389v1>

Submitted on 22 Aug 2021

HAL is a multi-disciplinary open access archive for the deposit and dissemination of scientific research documents, whether they are published or not. The documents may come from teaching and research institutions in France or abroad, or from public or private research centers.

L'archive ouverte pluridisciplinaire **HAL**, est destinée au dépôt et à la diffusion de documents scientifiques de niveau recherche, publiés ou non, émanant des établissements d'enseignement et de recherche français ou étrangers, des laboratoires publics ou privés.

Global forest carbon uptake due to nitrogen and phosphorus deposition from 1850 to 2100

Reference:

Wang Rong, Goll Daniel, Balkanski Yves, Hauglustaine Didier, Boucher Olivier, Ciais Philippe, Janssens Ivan, Penuelas Josep, Guenet Bertrand, Sardans Jordi,-
Global forest carbon uptake due to nitrogen and phosphorus deposition from 1850 to 2100
Global change biology - ISSN 1354-1013 - 23:11(2017), p. 4854-4872
Full text (Publisher's DOI): <https://doi.org/10.1111/GCB.13766>
To cite this reference: <https://hdl.handle.net/10067/1466540151162165141>

1 Global forest carbon uptake due to nitrogen and phosphorus deposition from
2 1850 to 2100

3

4 Rong Wang^{1,2,3}, Daniel Goll^{1,2}, Yves Balkanski^{1,2}, Didier Hauglustaine^{1,2}, Olivier Boucher⁴, Philippe
5 Ivan Janssens⁵, Josep Penuelas^{6,7}, Bertrand Guenet^{1,2}, Jordi Sardans^{6,7}, Laurent Bopp^{1,2}, Nicolas Vuichard¹,
6 Feng Zhou², Bengang Li², Shilong Piao², Shushi Peng², Ye Huang¹, Shu Tao²

7

8 ¹Laboratoire des Sciences du Climat et de l'Environnement, CEA CNRS UVSQ, 91190 Gif-sur-Yvette,
9 France ²Sino-French Institute for Earth System Science, College of Urban and Environmental Sciences,
10 Peking University, 100871 Beijing, China ³Department of Global Ecology, Carnegie Institution for Science,
11 Stanford, 94305 California, USA ⁴Laboratoire de Météorologie Dynamique, IPSL/CNRS, Université Pierre
12 et Marie Curie, 75252 Paris, France ⁵Department of Biology, University of Antwerp, Universiteitsplein 1,
13 B-2610 Wilrijk, Belgium ⁶CSIC, Global Ecology Unit CREAM-CSIC-UAB, Bellaterra, 08193 Catalonia,
14 Spain ⁷CREAF, Cerdanyola del Vallès, 08193 Catalonia, Spain

15

16 Correspondence to: Rong Wang (rong.wang@lsce.ipsl.fr)

17

18 **Abstract:**

19 **Spatial patterns and temporal trend of nitrogen (N) and phosphorus (P) deposition are important for**
20 **quantifying their impact on forest carbon (C) uptake. In a first step, we modeled historical and**
21 **change in the global distributions of the atmospheric deposition of N and P from the dry and wet**
22 **deposition of aerosols and gases containing N and P. Future projections were compared between two**
23 **scenarios with contrasting aerosol emissions. Modeled fields of N and P deposition and P**
24 **concentration were evaluated using globally distributed *in situ* measurements. N deposition peaked**
25 **around 1990 in European forests and around 2010 in East Asian forests, and both increased 7-fold**
26 **relative to 1850. P deposition peaked around 2010 in South Asian forests and increased 3.5-fold**
27 **relative to 1850. In a second step, we estimated the change in C storage in forests due to the**
28 **fertilization by deposited N and P ($\Delta C_{v\text{ dep}}$), based on the retention of deposited nutrients, their**
29 **allocation within plants, and C:N and C:P stoichiometry. $\Delta C_{v\text{ dep}}$ for 1997-2013 was estimated to be**
30 **$0.27 \pm 0.13 \text{ Pg C yr}^{-1}$ from N and $0.054 \pm 0.10 \text{ Pg C yr}^{-1}$ from P, contributing 9% and 2% of the**
31 **terrestrial C sink, respectively. Sensitivity tests show that uncertainty of $\Delta C_{v\text{ dep}}$ was larger from P**
32 **than from N, mainly due to uncertainty in the fraction of deposited P that is fixed by soil. $\Delta C_{P\text{ dep}}$ was**
33 **exceeded by $\Delta C_{N\text{ dep}}$ over 1960-2007 in a large area of East Asian and West European forests due to a**
34 **faster growth in N deposition than P. Our results suggest a significant contribution of anthropogenic**
35 **P deposition to C storage, and additional sources of N are needed to support C storage by P in some**
36 **Asian tropical forests where the deposition rate increased even faster for P than for N.**

37

38 1. Introduction

39 The processes controlling the terrestrial carbon (C) sink are a major source of uncertainty in projections of
40 the historical and future evolution of atmospheric CO₂ (Matthews, 2007; Ahlstrom *et al.*, 2012).
41 Observations and models both suggest that terrestrial C sinks are limited by nitrogen (N) and phosphorus (P)
42 with notable regional differences (Hungate *et al.*, 2004; Reich *et al.*, 2006; Elser *et al.*, 2007; Thornton *et*
43 *al.*, 2009; Norby *et al.*, 2010; Vitousek, *et al.*, 2010; Goll *et al.*, 2012, Penuelas *et al.*, 2013,
44 Fernández-Martínez *et al.*, 2014; Wieder *et al.*, 2015). The majority of studies predict a large limitation of
45 the C sink in the 21st century due to limited availabilities of N and P, but the extent of this limitation varies
46 widely among studies. This effect of limitation implies that terrestrial C sinks are sensitive to the inputs of
47 N and P from atmospheric deposition in the case of non-cultivated ecosystems. In particular, anthropogenic
48 emissions of reactive N, including oxidized (*e.g.* NO_x) and reduced (*e.g.* NH₃) N have increased
49 significantly in the past decades (Galloway *et al.*, 2004), causing notable change in N availability in
50 northern temperate and boreal forests (Magnani *et al.*, 2007) and more recently in tropical forests (Hietz *et*
51 *al.*, 2011). During 1982-2009, N deposition has contributed 9% to the observed greening of the Earth (Zhu
52 *et al.*, 2016).

53 Atmospheric deposition increases the availability of N and P, and thus should increase or sustain the
54 terrestrial C sink (Graham and Duce, 1979; Galloway *et al.*, 2004; Okin *et al.*, 2004; Mahowald, 2011).
55 Nadelhoffer *et al.* (1999) estimated that N deposition accounts for a C sink of 0.25 Pg C yr⁻¹ in 1990s based
56 on ¹⁵N tracer studies in nine forests and a prescribed N input of 5.1 Tg N yr⁻¹ to the Earth's forests. For the
57 same period, Liu and Greaver (2009) estimated a somewhat larger contribution of N deposition to the
58 global terrestrial C sink of 0.35-0.58 Pg C yr⁻¹ based on a meta-analysis of field observations. Thomas *et al.*
59 (2010) attributed a C sink of 0.31 Pg C yr⁻¹ to this factor in forests by comparing forest growth rates for
60 different exposures of N deposition during the 1980s and 1990s based on data from the national forest
61 inventory in the USA. Zaehle *et al.* (2010, 2014) estimated that N deposition resulted in a net terrestrial C
62 sink of 0.2 Pg C yr⁻¹ during 1996-2005 using an OCN process-based vegetation model. de Vries *et al.*
63 (2014) estimated a contribution of comparable magnitude (0.2-0.5 Pg C yr⁻¹) from N deposition to the
64 global land C sink using a stoichiometric approach. While the impact of atmospheric N deposition on
65 terrestrial C sink has been assessed by several studies, the contribution of P deposition has not yet been
66 quantified. This is because reconstruction of historical changes in P deposition are lacking.

67 Several studies have attempted to simulate the spatial distributions of N deposition (Holland *et al.*, 1997;
68 Lamarque *et al.*, 2005, 2013; Dentener *et al.*, 2006; Phoenix *et al.*, 2006; Paulot *et al.*, 2013; Hauglustaine
69 *et al.*, 2014) and P deposition (Mahowald *et al.*, 2008) under current and future conditions driven by
70 emission inventories. These studies differ by their emission inventories, aerosol chemistry and horizontal
71 resolutions of chemical transport models (CTM) (Table S1). However, the modeled N and P deposition
72 rates are subject to high uncertainty, which remains unquantified. For example, the modeled wet deposition
73 rates of nitrate (NO₃) and ammonium (NH₄) as means of 11 CTMs were underestimated by 40-140%
74 compared to atmospheric station data depending on the region (Lamarque *et al.*, 2013). Hauglustaine *et al.*
75 (2014) suggested that the underestimation in wet N deposition for Asia in their CTM is of 50-60% due to a

76 bias in the region's N emissions estimates and the model's coarse horizontal resolution. Earlier estimates of
77 present day total P deposition (Mahowald *et al.*, 2008) were underestimated by almost one order of
78 magnitude, likely due to an underestimation of the contribution of human activities to P emissions (Wang *et al.*,
79 2015a). Recent measurements in China underline the anthropogenic component of P deposition
80 showing that the bulk deposition of P followed a power-law increase with decreasing distance of
81 monitoring sites to the nearest cities (Du *et al.*, 2016). More measurements over a wide range of
82 representative stations are necessary to confirm the regional contribution of combustion sources to P in the
83 atmosphere. High-resolution data sets of modeled N and P deposition over forests supported by global
84 measurements are critical for understanding the C sink that offsets the increase in fossil-fuel C emissions
85 and the limitations of primary productivity by N and P. However, such data sets are not available due to
86 uncertainties in the emission inventories of N and P and limited understanding of N chemistry in aerosols.

87 Elemental stoichiometry has been used to identify major constraints in the change in C storage by terrestrial
88 ecosystems due to nutrients either available in soils or deposited from the atmosphere, based on
89 assumptions about the allocation of nutrients and their elemental ratios (e.g., C:N or C:P) in ecosystemic C
90 pools. This method assumes that N and P limitation of net primary productivity (NPP) is widespread across
91 global biomes (Elser *et al.*, 2007). For example, Cleveland *et al.* (2013) used this method to show that
92 external inputs of N and P through atmospheric deposition supports 3.8% and 16% of new NPP, but the
93 uncertainty has not been considered. De Vries *et al.* (2014) used this method to infer that N deposition
94 supports a global forest C sink of 0.28-0.45 Pg C yr⁻¹ by assuming that 15% of deposited N is retained in
95 forest biomass and 15% in soil in tropical forests, but the impact of P was not considered in this study.

96 Our study aims to fill these gaps by providing the first time-series of N & P deposition and the resulting C
97 sink taking into account the major sources of uncertainty. To do so, we calculated the temporal evolutions
98 of N and P deposition in a CTM prescribed by reconstructions of historical and future scenarios of
99 anthropogenic emissions and evaluated the so derived N wet deposition, P total deposition and surface P
100 concentrations in aerosols with in situ measurements. We built a modeling framework to estimate the C
101 sequestration of global forests due to historical and future N and P deposition. We accounted for
102 uncertainties in the stoichiometric and allocation parameters by employing a Monte Carlo method in a
103 stoichiometric mass-balance approach, and identify key factors influencing the forest C sequestration.

104 **2. Materials and methods**

105 **2.1. Atmospheric deposition of N and P for 1850-2100**

106 The global aerosol chemistry climate model LMDZ-INCA couples the LMDz (Laboratoire de
107 Météorologie Dynamique, version-4) General Circulation Model (Hourdin *et al.*, 2006) and the INCA
108 (INteraction with Chemistry and Aerosols, version-4) aerosol module (Hauglustaine *et al.*, 2014). A full
109 description of the model is provided in the **Supporting Information**. To run the model, emissions data
110 included sea-salt and dust for P, primary biogenic aerosol particles for P, oceanic emissions for N (NH₃),
111 vegetation emissions for N (NO), agricultural activities (including fertilizer use and livestock) for N, and
112 fuel combustion for both N (NO_y and NH_x) and P. Regarding N-containing aerosols and gases,

113 LMDZ-INCA was run with a fully interactive atmospheric N cycle (Hauglustaine *et al.*, 2014) at a
114 horizontal resolution of 1.27° latitude by 2.5° longitude with 39 vertical layers in the atmosphere to
115 simulate the global dry and wet deposition of NO_y and NH_x for 1850, 1960, 1970, 1980, 1990, 1997-2013,
116 2030, 2050 and 2100. The same resolution is used for the transport and deposition of P aerosols in
117 LMDZ-INCA with the emission data provided by Wang *et al.* (2015a), which are transported in three size
118 bins for P emitted by combustion processes with a diagnostic mass median diameter (MMD) of 0.14, 2.5
119 and 10.0 μm, one size bin for P from primary biogenic aerosol particles (MMD=5.0 μm), one size bin for P
120 from mineral dust (MMD=2.5 μm), and three size bins for P from marine sea-salt particles (Balkanski *et al.*,
121 2011). Meteorological fields from a reanalysis of the European Centre for Medium-Range Weather
122 Forecasts (ECMWF) have been used in the present configuration to nudge the model transport and removal
123 processes for 1980 and 1990 and for each year during the recent 1997-2013 period. Additional simulations
124 were performed with emissions for 1850, 1960, 1970 and into the future all using meteorological fields for
125 2005.

126 The emissions prescribed to LMDZ-INCA were obtained from published data sets or emission inventories.
127 We focused on generating coherent emission data sets for all species, and the methods are fully described
128 in the **Supporting Information. Table S2** lists the emission data sets used in our study. In brief, global
129 0.5°×0.5° emissions of NO_x, NH₃, sulfur dioxide (SO₂), non-methane volatile organic compounds
130 (NMVOCs), methane (CH₄), carbon monoxide (CO), organic carbon (OC) and black carbon (BC) for 2005,
131 2010 and 2030 were obtained from the ECLIPSE.GAINS.4a model (Klimont *et al.*, 2013). SO₂, CO, CH₄
132 and NMVOCs species should be treated consistently with N aerosols, because they influence N chemistry
133 in the model (Hauglustaine *et al.*, 2014). The ECLIPSE.GAINS.4a emissions of all species were extended
134 to other years of simulations using historical data from the ACCMIP and MACCity inventories (Lamarque
135 *et al.*, 2010; Granier *et al.*, 2011) and future data from the RCP4.5 and RCP8.5 scenarios by Lamarque *et al.*
136 (2011). In addition, natural emissions of NO and NH₃ from soil (Bouwman *et al.*, 1997; Lathière *et al.*,
137 2006) were assumed to be constant throughout the period; natural oceanic emissions of NH₃ were
138 calculated in the INCA model following the formulations proposed by Paulot *et al.* (2015), with monthly
139 2°×2° fields of surface sea-water concentrations of NH₄, pH and salinity as simulated by the oceanic
140 biogeochemical model PISCES (Wang *et al.*, 2015b). Emissions of P from fossil fuels and biofuel were
141 estimated annually for 1960 to 2007 (Wang *et al.*, 2015a), which were extended to other years of
142 simulations. Natural emissions of P from mineral dust, primary biogenic aerosol particles, sea salt and
143 volcanoes were assumed to be constant (Wang *et al.*, 2015a). All N and P emissions from fossil fuels,
144 biofuel and agricultural activities were assumed to be constant throughout each year without seasonal
145 variation. Monthly 0.5°×0.5° gridded emissions by natural or anthropogenic (deforestation) burning of
146 biomass were generated for 1997-2013 from the GFED4.1 inventory (Giglio *et al.*, 2013) and for other
147 years from the ACCMIP inventory (Lamarque *et al.*, 2010). Emissions from biomass burning for 2030,
148 2050 and 2100 were assumed to be the same as the averages for 2010-2013. We only analyzed the changes
149 of future N and P deposition from anthropogenic sources due to the lack of estimates of natural emissions,
150 but both natural and anthropogenic sources were included for evaluating modeled N and P deposition

151 against measurements.

152 **2.2. Observed N and P deposition rates and P concentrations**

153 To evaluate the modeled N and P deposition rates, we used three observational data sets (**Figure S1**),
154 including (i) a recent global data set of wet N deposition rates measured during 2002-2006 ([Vet et al.,](#)
155 [2014](#)), (ii) a recent global data set of total P deposition rates measured during 1960-2010 ([Tippling et al.,](#)
156 [2014](#)), and (iii) a recent global data set of surface P deposition concentrations measured during 1960-2008
157 ([Mahowald et al., 2008](#)). Dry N deposition was not evaluated due to the lack of data, similar to previous
158 studies ([Larmarque et al., 2005](#); [Dentener et al., 2006](#)). Before using these observational data for model
159 evaluation, we have further collected data to increase coverage of wet N deposition data in South America
160 and Africa, removed some data of total P deposition with a high potential for contamination, and divided
161 the measured surface P concentrations into short-term and long-term measurements. A full description is
162 provided in the **Supporting Information**.

163 **2.3. Additional C fixation attributable to N and P deposition**

164 **2.3.1. A stoichiometric method**

165 A stoichiometric mass balance approach was used to estimate the change in C storage attributable to N and
166 P deposition over global forests, based on the fraction of deposited nutrients retained in the ecosystems and
167 incorporated into biomass and soil carbon pools ([Nadelhoffer et al., 1999](#); [Cleveland et al., 2013](#); [de Vries](#)
168 [et al., 2014](#); [Wieder et al., 2015](#)). We distinguished between four biomass C pools (leaves, stems, fine roots
169 and coarse roots; each with different stoichiometry) and one soil C pool. Five types of forests are
170 considered, namely deciduous broadleaf, deciduous needle-leaf, evergreen broadleaf, evergreen needle-leaf
171 and mixed forests. The global land cover data set at a spatial resolution of 1 km ([Hansen et al., 2000](#)) for
172 the year 2010, as a product of Moderate Resolution Imaging Spectroradiometer (MODIS), was used to map
173 these five types of forests. Forest areas have changed significantly since 1850 ([Foley et al., 2005](#); [Houghton](#)
174 [et al., 2003](#)). Here, we applied the fixed forest cover map by Hansen *et al.* (2000) in the calculation of $\Delta C_{v, \text{dep}}$
175 throughout the period of 1850-2100. The uncertainty induced by assuming a fixed forest cover map on
176 $\Delta C_{v, \text{dep}}$ is quantified in **Section 3.7**. To do this, we re-calculated $\Delta C_{v, \text{dep}}$ with the variable forest cover map
177 for 1850-2010 according to the reconstruction of ([Peng et al., 2017](#)) and the fraction of five types of forests
178 within each $1^\circ \times 1^\circ$ grid from Hansen *et al.* (2000).

179 We assumed that in 1850 the forest C stocks were in equilibrium with the pre-industrial N and P deposition
180 levels (i.e. $\Delta C_{v, \text{dep}} = 0$), so that only the change in N and P deposition relative to the background levels can
181 cause an extra forest C storage, allowing our estimates to cover the additional N and P emissions from
182 fossil fuels and biofuel burning, atmospheric NH_3 and NO_x emissions from agriculture, and change in N
183 and P emissions from biomass burning compared to 1850. Hence our analysis included the wind export of
184 P from croplands and savanna to forests through fire emissions and atmospheric transport. It should be
185 noted that direct anthropogenic effects on fires (*e.g.*, fire suppression and land use change) and indirect
186 anthropogenic effects (*e.g.*, changes in climate affecting fire regimes) were not explicitly distinguished in
187 the historical fire emission inventory we used ([Giglio et al., 2013](#)). In addition, although our calculation of

188 $\Delta C_{v\text{ dep}}$ covers C storage due to N and P from anthropogenic fires, we did not try to estimate the C
 189 emissions from these anthropogenic fires which are always termed as part of C emissions from land-use
 190 change in global C budget (Le Quere *et al.*, 2016). However, we did not account for the change of
 191 atmospheric CO₂ concentrations, climate and forest cover change (Hansen *et al.*, 2013).

192 In each pixel at a spatial resolution of 1°×1°, additional forest C storages supported by anthropogenic N or
 193 P deposition ($\Delta C_{v\text{ dep}}$, where v stands for either N or P) were expressed as:

194

$$\Delta C_{N\text{ dep}_i}(t) = f_{N_{veg}} a_{N_i} s_{N_i} [d_N(t) - d_N(1850)] \quad (1)$$

195

$$\Delta C_{P\text{ dep}_i}(t) = f_{P_{veg}} a_{P_i} s_{P_i} [d_P(t) - d_P(1850)] \quad (2)$$

196 where i is biomass pool ($i = 1$ for leaves, 2 for stems, 3 for fine roots and 4 for coarse roots), $f_{N_{veg}}$ and $f_{P_{veg}}$
 197 are the retention fractions of deposited N and P in biomass pools, respectively, a_{N_i} and a_{P_i} are the allocation
 198 fractions of N and P in each pool, respectively, s_{N_i} and s_{P_i} are the C:N and C:P stoichiometric ratios,
 199 respectively, and $d_N(t)$ and $d_P(t)$ are the deposition rates of N and P for year t , respectively. All deposition
 200 fields and land cover fractions were re-interpolated to the 1°×1° grid for the calculation of $\Delta C_{v\text{ dep}}$.

201 Similarly, in each pixel, the $\Delta C_{v\text{ dep}}$ realized in soil were expressed as:

202

$$\Delta C_{N\text{ dep}_{soil}}(t) = f_{N_{soil}} s_{N_{soil}} [d_N(t) - d_N(1850)] \quad (3)$$

203

$$\Delta C_{P\text{ dep}_{soil}}(t) = f_{P_{soil}} s_{P_{soil}} [d_P(t) - d_P(1850)] \quad (4)$$

204 where $f_{N_{soil}}$ and $f_{P_{soil}}$ are the retention fractions of N and P in soil, respectively, and $s_{N_{soil}}$ and $s_{P_{soil}}$ are the C:N
 205 and C:P stoichiometric ratios in soil biota, respectively.

206 There are two limitations in our approach. First, like de Vries *et al.* (2014), we approximate a time scale of
 207 10-20 years for the $\Delta C_{v\text{ dep}}$, because ecosystems take time to sequester C in forest biomass and soil after an
 208 initial disturbance (Goulden *et al.*, 2011), such as the level of N and P deposition for most of the global
 209 forests. It should be noted that our stoichiometric mass-balance model cannot resolve processes governing
 210 the C storage changes attributed to deposition on shorter timescales. It is likely that the instantaneous effect
 211 at the early stage of forest succession (e.g., less than 5 years) is lower, due to enhancement of soil C
 212 decomposition by N deposition (Goulden *et al.*, 2011). Second, different turnover times of the plant and
 213 soil pools should influence the C response to deposition, which is not included in our model. According to
 214 de Vries *et al.* (2014), the C storage in the woody biomass (stem and coarse root) determines C
 215 sequestration by forest trees, while the C storage in the non-woody biomass (leaves and fine root), which is
 216 fast-turnover (Iversen *et al.*, 2017), determines C sequestration in soil. We estimated the sum of them based
 217 on the allocation of the deposited nutrient in different pools measured at a time scale of around 2-9 years
 218 (Schlesinger, 2009). At longer time periods, the C sequestration is determined by other disturbances, such
 219 as forest fires and forest harvesting, which is not considered in our study. More knowledge gained in
 220 database analyses for nutrient use in the tree growth (e.g., Sardans and Peñuelas, 2013, 2015) would enable
 221 us to better understand these processes in future process-based ecosystem models.

222 Although $\Delta C_{v\text{dep}}$ account for C storage supported by deposited nutrients on timescales of 10-20 years (de
 223 Vries *et al.*, 2014), it should be noted that a fraction of deposited N and P may still contribute to $\Delta C_{v\text{dep}}$
 224 beyond the 10-20 year timeframe. This impact is small for $\Delta C_{N\text{dep}}$, because a large fraction of N is lost by
 225 denitrification or leaching. The impact for $\Delta C_{P\text{dep}}$, however, is not negligible, because P is mostly fixed by
 226 the soil and is less prone to loss. We estimated $\Delta C_{P\text{dep}}$ by fixing an “effective fraction” of the deposited P (f_{fix})
 227 to account for this impact (see **Section 2.3.2**).

228 All parameters were determined with central values and uncertainty ranges (see **Section 2.3.2, 2.3.3, and**
 229 **2.3.4**). In brief, the parameters $f_{N\text{veg}}$, $f_{P\text{veg}}$, a_i , s_{Ni} , s_{Pi} , $f_{N\text{soil}}$ and $f_{P\text{soil}}$ were derived for deciduous broadleaf,
 230 deciduous needle-leaf, evergreen broadleaf, evergreen needle-leaf and mixed forests; parameters values and
 231 their uncertainty ranges are summarized in **Table 1**. Uncertainties in the modeled deposition rates (d_N and
 232 d_P) were derived from a comparison with the available observation data sets (see **Section 3.2**).

233 **Table 1.** Parameters used to estimate carbon fixation due to anthropogenic N and P deposition in forests.
 234 The 95% confidential intervals adopted as the lower and upper estimates for each parameter applied in our
 235 Monte Carlo simulations are in parentheses.

Forest type	Evergreen needleleaf forest	Evergreen broadleaf forest	Deciduous needleleaf forest	Deciduous broadleaf forest	Mixed forest
C:N (g C: g N)					
Leaves	42 (34-50)	21 (17-25)	50 (40-60)	21 (17-25)	28 (22-34)
Stems	250 (200-300)	150 (120-180)	250 (200-300)	175 (140-210)	175 (140-210)
Fine roots	78 (62-94)	78 (62-94)	41 (33-49)	41 (33-49)	41 (33-49)
Coarse roots	250 (200-300)	150 (120-180)	250 (200-300)	175 (140-210)	175 (140-210)
Soil	31 (28-35)	16 (14-18)	20 (18-21)	19 (18-20)	19 (18-20)
C:P (g C: g P)					
Leaves	408 (326-490)	400 (320-480)	405 (324-486)	333 (266-400)	278 (222-334)
Stems	3750 (3000-4500)	2250 (1800-2700)	3750 (3000-4500)	2625 (2100-3150)	2625 (-)
Fine roots	1170 (936-1404)	1020 (816-1224)	615 (492-738)	615 (492-738)	615 (492-738)
Coarse roots	3750 (3000-4500)	2250 (1800-2700)	3750 (3000-4500)	2625 (2100-3150)	2625 (2100-3150)
Soil	1030 (459-2312)	169 (134-214)	318 (214-472)	391 (306-500)	254 (214-300)
Retention fractions of N and P in plants					
$f_{N\text{veg}}$	0.23 (0.14-0.30)	0.15 (0.10-0.20)	0.23 (0.14-0.30)	0.23 (0.14-0.30)	0.23 (0.14-0.30)
$f_{P\text{veg}}$	0.05 (0.016-0.22)	0.09 (0.027-0.36)	0.05 (0.016-0.22)	0.05 (0.016-0.22)	0.05 (0.016-0.22)
Retention fractions of N and P in soil					
$f_{N\text{soil}}$	0.52 (0.26-0.78)	0.15 (0.10-0.20)	0.52 (0.26-0.78)	0.52 (0.26-0.78)	0.52 (0.26-0.78)
$f_{P\text{soil}}$	0.13 (0.038-0.50)	0.09 (0.03-0.36)	0.13 (0.038-0.50)	0.13 (0.038-0.50)	0.13 (0.038-0.50)
Allocation fraction of N (a_{Ni})					
Leaves	0.42	0.56	0.42	0.49	0.46
Stems	0.34	0.22	0.34	0.33	0.34
Fine roots	0.16	0.17	0.16	0.11	0.13

Coarse roots	0.08	0.05	0.08	0.07	0.07
Allocation fraction of P (a_{Pi})					
Leaves	0.32	0.63	0.28	0.50	0.35
Stems	0.40	0.19	0.42	0.32	0.40
Fine roots	0.19	0.13	0.20	0.11	0.16
Coarse roots	0.09	0.04	0.10	0.07	0.09

236

237 Sensitivity tests were performed to quantify the influence of the major parameters on the $\Delta C_{v\text{dep}}$ by N and
 238 P (see **Section 3.4**). Finally, Monte Carlo simulations were applied to estimate the central values of $\Delta C_{v\text{dep}}$
 239 in global forests and to estimate their uncertainties in each pixel at a spatial resolution of $1^\circ \times 1^\circ$. In brief,
 240 the model was run 10000 times by drawing input parameters from uniform or normal uncertainty
 241 distributions of model parameter and N- and P-deposition rates. The medians and 95% confidence intervals
 242 (CI) were used to represent the central estimate and the associated uncertainty, respectively, based on the
 243 Monte Carlo simulations.

244 **2.3.2. Retention of N and P in the ecosystems**

245 Schlesinger (2009) reported a median N retention fraction of 23% (with an interquartile range of 14-30%)
 246 for biomass pools ($f_{N\text{veg}}$) and 52% (with an interquartile range of 26-78%) for soils ($f_{N\text{soil}}$) in boreal and
 247 temperate forests. De Vries *et al.* (2007) suggested a lower N-retention fraction of 15% (with a 90%
 248 uncertainty range of 10-20%) for both $f_{N\text{veg}}$ and $f_{N\text{soil}}$ in tropical forests. We adopted these median estimates
 249 and their uncertainty ranges. The non-retained fraction of deposited N lost by leaching, volatilization and
 250 denitrification is not explicitly modeled.

251 Evidence suggests that N inputs from atmospheric deposition can be taken up by forest canopies (Sievering
 252 *et al.*, 2007; Gaige *et al.*, 2007; Sparks, 2009). De Vries *et al.* (2014), however, suggested that the effect of
 253 uptake of N by canopies on C fixation is likely to be small, because a small fraction of canopy-retained N is
 254 absorbed and used in leaves. Gaige *et al.* (2007) suggested that denitrification and nitrification do not occur
 255 in the canopy, despite a high retention fraction of N deposition in the canopy. Sparks (2009) suggested that
 256 foliar uptake of reactive N should be considered separately from soil-deposited N, but pointed out that it is
 257 difficult to link canopy uptake of N directly to assimilation. Dail *et al.* (2009) found that only 3-6% of the
 258 labeled ^{15}N recoverable in plant biomass was recovered in live foliage and bole wood and that tree twigs,
 259 branches and bark were the major sinks (50%) after 2 years of NH_4NO_3 addition. We therefore did not
 260 account for this process in our central case, following the suggestion by de Vries *et al.* (2014), but discuss
 261 the potential impact in a sensitivity test in **Section 4.2**.

262 The fate of deposited P in ecosystems differs from that of N. First, P is less mobile than N in soils (Aerts
 263 and Chapin, 2000), so the fractional P loss by leaching is smaller than for N. Second, denitrification has no
 264 counterpart for gaseous P loss to the atmosphere. Third, the physical fixation of P and its eventual
 265 occlusion in soil reduces the availability of deposited P to leaching and uptake by plants and microbes. The
 266 fate of deposited P in forests has unfortunately not yet been measured, to the best of our knowledge, and

267 was estimated in our study based on two assumptions. First, we assumed that 10% of the deposited P was
 268 directly lost by runoff as Sattari *et al.* (2012) assumed for fertilizer P. Second, by assuming that P
 269 deposition input to soil is much smaller than the actual stocks of labile and stable P in soil and thus does not
 270 affect the stock size, we approximated the fixation of an “effective fraction” of deposited P ($f_{P_{fix}}$),
 271 corresponding to the net transfer of P between ‘labile’ and ‘stable’ forms, based on transfer coefficients
 272 (μ_{SL} and μ_{LS}) between stable and labile P:

$$273 \quad f_{P_{fix}} = 1 - \mu_{SL}/\mu_{LS} \quad (5)$$

274 We used μ_{SL} and μ_{LS} to derive a central estimate of $f_{P_{fix}}$ (80%) but a wide range of uncertainty (20% to 94%)
 275 as recommended by Sattari *et al.* (2012). We also assumed that the fraction of ecosystem-retained P taken
 276 up by plants ($f_{P_{uptake}}$) was the same as that of N, at 30% for boreal and temperate forests and 50% for tropical
 277 forests (Schlesinger, 2009; de Vries *et al.*, 2007), due to lack of direct measurements of the fraction of
 278 ecosystem-retained P taken up by plants. We then derived the retention of P in vegetation ($f_{P_{veg}}$) and soil ($f_{P_{soil}}$)
 279 using $f_{P_{fix}}$, $f_{P_{loss}}$ and $f_{P_{uptake}}$:

$$280 \quad f_{P_{veg}} = (1 - f_{P_{loss}})(1 - f_{P_{fix}})f_{P_{uptake}} \quad (6)$$

$$281 \quad f_{P_{soil}} = (1 - f_{P_{loss}})(1 - f_{P_{fix}})(1 - f_{P_{uptake}}) \quad (7)$$

282 We estimated that $f_{P_{veg}}$ was 5.4% (1.6-22% as the uncertainty range) and $f_{P_{soil}}$ was 13% (3.8-50% as the
 283 uncertainty range) in boreal and temperate forests and that $f_{P_{veg}}$ was 9.0% (2.7-36% as the uncertainty range)
 284 and $f_{P_{soil}}$ was 9.0% (2.7-36% as the uncertainty range) in tropical forests (**Table 1**).

285 **2.3.3. Allocation of N and P in plants**

286 We used the values of a_{Ni} diagnosed by de Vries *et al.* (2014) for deciduous broadleaf, evergreen broadleaf
 287 and needleleaf forests. The a_{Ni} averaged over deciduous broadleaf and needleleaf forests was applied for
 288 mixed forests (**Table 1**). The uncertainty associated with a_{Ni} , however, was not provided and was estimated
 289 below. The C:N ratio differs for woody (stem and coarse root) and non-woody (leaf and fine root) pools, so
 290 the assumption that uncertainties in a_{Ni} are the same as the uncertainties associated with the fraction of N
 291 allocated to the woody component is reasonable. A meta-analysis of ^{15}N addition experiments suggested
 292 that 53% of total N uptake is allocated to woody biomass (Templer *et al.*, 2012), compared to 25% reported
 293 by Nadelhoffer *et al.* (1999). This latter low value is 7-40% lower than that used in our study, and the high
 294 value is 26-96% higher than the central value used in our study (**Table 1**). We accordingly applied two half
 295 normal distributions to cover the uncertainty of a_{Ni} .

296 We are not aware of any experiment measuring the allocation of deposited P to different biomass pools, so
 297 we derived the allocation fractions of P and their uncertainties from the allocation of N and the
 298 stoichiometric ratios of these two elements as:

$$299 \quad a_{P_i} = \frac{a_{N_i} \cdot s_{N_i} / s_{P_i}}{\sum_{i=1}^4 (a_{N_i} \cdot s_{N_i} / s_{P_i})} \quad (8)$$

300 where s_{N_i} and s_{P_i} are the C:N and C:P stoichiometric ratios, respectively, in each pool of the plant.

301 **2.3.4. C:N and C:P stoichiometric ratios in different pools**

302 C:N and C:P stoichiometric ratios in soil and their 95% CI were derived from a global data set of the
303 nutrient composition of soil (Xu *et al.*, 2013). The median C:N and C:P stoichiometric ratios of leaves,
304 stems, fine roots and coarse roots were obtained from Cleveland *et al.* (2013). Wang *et al.* (2010) suggested
305 that the minimum and maximum of C:N and C:P stoichiometric ratios were $\pm 20\%$ relative to the means,
306 which we applied as uncertainties for s_{N_i} and s_{P_i} .

307 2.4. Maximum and minimum effects of N and P deposition

308 The change in C fixation due to nutrients addition in an ecosystem can be approximated based on the most
309 limiting element (Vitousek *et al.*, 1984, 2010), but the stoichiometric mass balance approach we used could
310 not identify the most limiting element. Therefore, we estimated the maximum and minimum effects of $\Delta C_{v \text{ dep}}$
311 due to anthropogenic N and P deposition to characterize the degree of limitation by one of the two
312 elements. Accordingly, the minimum effects of anthropogenic N and P deposition yields a lower estimate
313 as:

$$314 \quad \Delta C_{v \text{ dep}}^{\min} = \min[\Delta C_{N \text{ dep}}, \Delta C_{P \text{ dep}}] \quad (9)$$

315 and the maximum effects of N and P deposition yields an upper estimate as:

$$316 \quad \Delta C_{v \text{ dep}}^{\max} = \max[\Delta C_{N \text{ dep}}, \Delta C_{P \text{ dep}}] \quad (10)$$

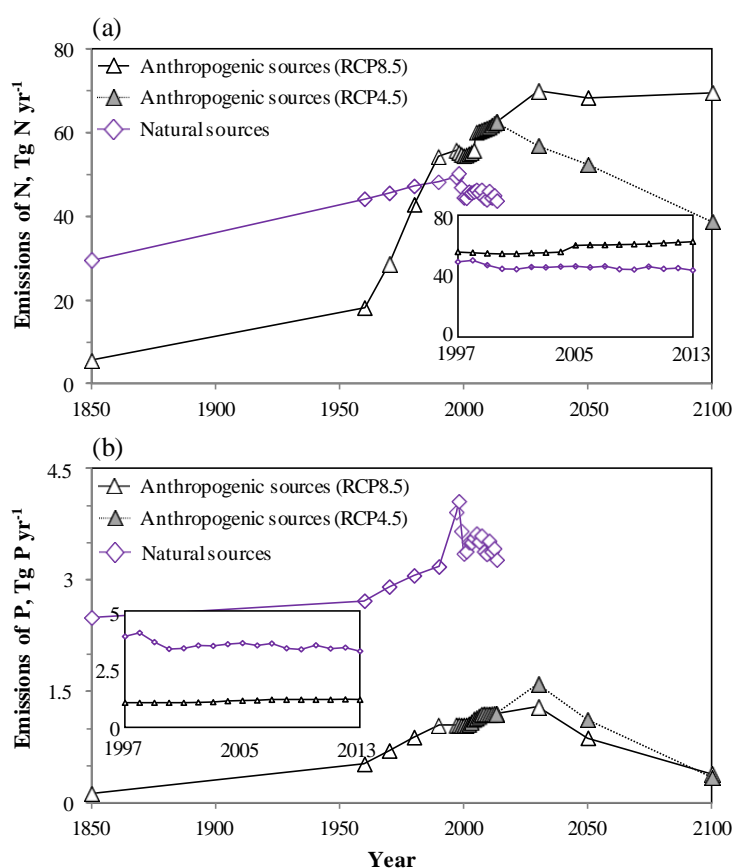
317 The minimum and maximum effects calculated here should be interpreted with caution. First, the minimum
318 effect is based on a hypothesis that the element with a lower capacity to fix C by deposition is more
319 limiting and that there is no additional source of this element than atmospheric deposition to support a
320 larger C storage. The difference between the effect by an element alone and the minimum effect denotes
321 the limitation by the other element that is enhanced by the deposition. Second, the maximum effect is based
322 on a hypothesis that the element with a higher capacity to fix C by deposition is more limiting and there is
323 enough of the other element to allow for the largest C storage. The difference relative to the effect by an
324 element alone denotes the limitation by the other one that is alleviated by the deposition. Regarding
325 uncertainties in the limitations by N and P, the combined effect of N and P deposition should fall between
326 the minimum and maximum effects. Although we cannot rule out that there are synergistic “additive”
327 effects (Elser *et al.*, 2007) as well as strictly negative effects (Penuelas *et al.*, 2013), such effects are rather
328 unlikely to occur in wide ranges of ecosystems and deposition loads. In addition, difference between the
329 maximum and minimum effect quantifies an imbalance between N and P induced by the deposition
330 providing that other sources of N and P were held constant. However, it should be noted that our
331 calculation does not account for the interaction between N and P cycles implied by recent studies. For
332 example, increasing N deposition can affect availability, uptake and using efficiency of P by altering
333 mycorrhizal activity, phosphatase enzymes and soil properties (Compton and Cole, 1998; Rowe *et al.*, 2008;
334 Marklein and Houlton, 2012; Lü *et al.*, 2013).

335 3. Results

336 3.1. N and P emissions

337 Natural and anthropogenic global emissions of N and P were estimated or derived for the past time slices in

338 1850-1990, for each year in 1997-2013 and for the future time slices in 2030-2100 (Figure 1). Total
 339 reactive-N emissions increased from 35 Tg N yr⁻¹ in 1850 to an average of 104 Tg N yr⁻¹ for 1997-2013,
 340 and were predicted to reach 83 and 114 Tg N yr⁻¹ by 2100 under the RCP4.5 and RCP8.5 scenarios,
 341 respectively. N emissions as the oxidized (NO_x) and reduced (NH₃) forms are listed in Table S3, which are
 342 close to previous estimates (Holand *et al.*, 1997; Galloway *et al.*, 2004; Lamarque *et al.*, 2005; Dentener *et al.*,
 343 2006; Paulot *et al.*, 2013). The main drivers of the increase in historical N emissions were a rapid rise in
 344 the use of fossil fuels, both the expansion and intensification of agricultural fertilization and an increase in
 345 the number of livestock (Schlesinger, 2009). N emissions from fossil fuel, biofuel and agricultural activities
 346 increased from 5.6 Tg N yr⁻¹ in 1850 (Lamarque *et al.*, 2010) to 60 Tg N yr⁻¹ in 2005 (Klimont *et al.*, 2013).
 347 The increase in reactive-N emissions was equivalent to twice the background N emissions in 1850. The
 348 emissions of P increased from 2.6 to 4.0 Tg P yr⁻¹ from 1850 to 2013, equivalent to a 57% increase relative
 349 to the background 1850 emissions. 47%, 25% and 28% of the increase in P emissions were from increases
 350 in emissions from fossil fuels, biofuel and deforestation fires, respectively. The N:P ratio in the emissions
 351 nearly doubled from 25 (on a molar basis) in 1850 to 48 in 2013 due to a faster growth of N than P
 352 emissions as outlined in a previous study (Peñuelas *et al.*, 2013).



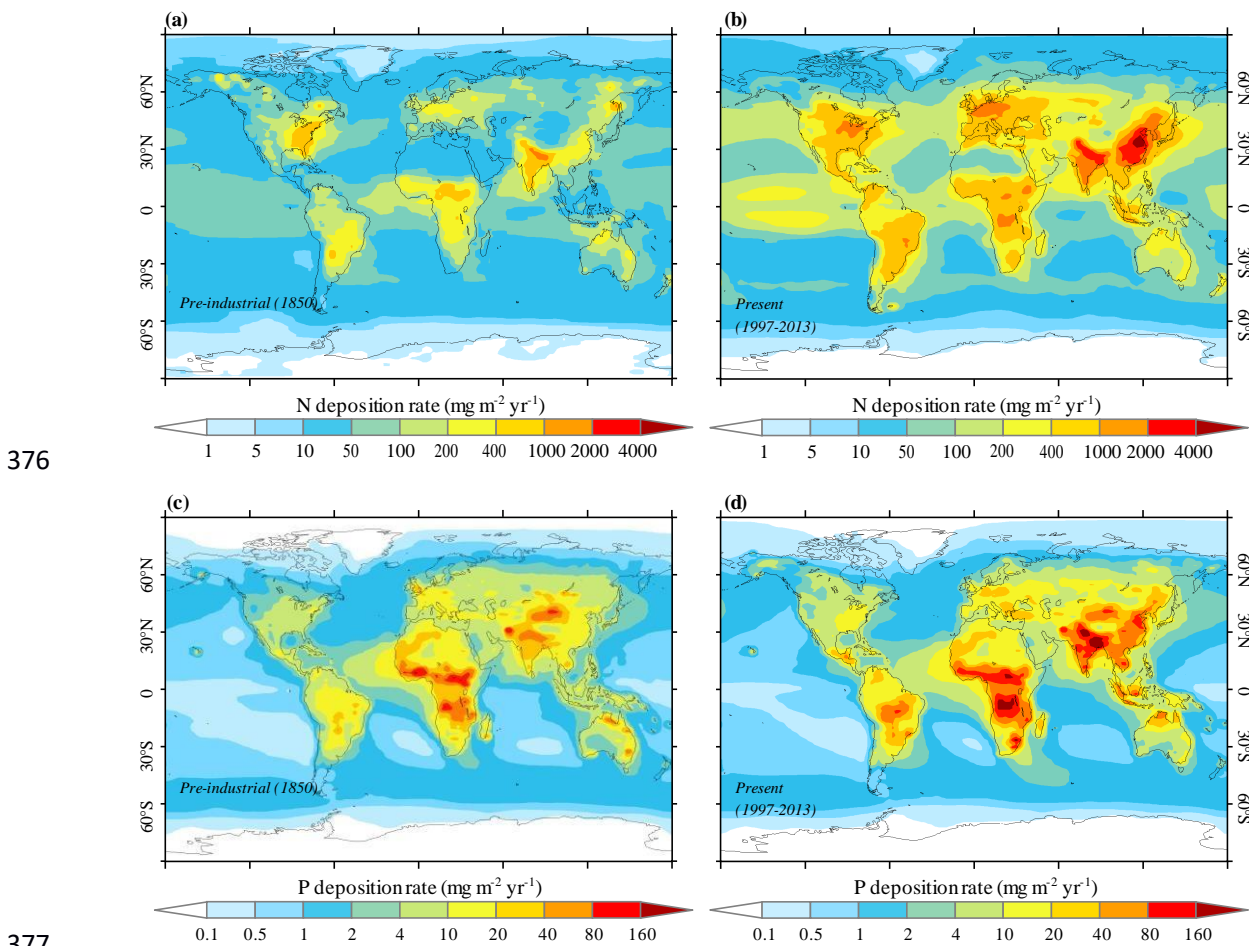
353
 354 **Figure 1.** (a) Global atmospheric N emissions. Anthropogenic sources include fossil fuels, biofuel and
 355 agricultural activities. Natural sources include NO_x and NH₃ emissions from biomass burning, NO_x and
 356 NH₃ emissions from soil, and NH₃ emissions from oceans. (b) Global atmospheric P emissions.
 357 Anthropogenic sources include fossil fuels and biofuel. Natural P sources include biomass burning, dust,
 358 sea salt, volcano particles and primary biogenic aerosol particles. The inset demonstrates the inter-annual
 359 recent variation over the period 1997-2013.

360

361 The future emissions of N differed considerably between the RCP4.5 and RCP8.5 scenarios, but the
362 emissions of P were similar. NH_3 emissions in 2100 will be 54% under the RCP8.5 than the RCP4.5
363 scenario, due to increased agricultural activities needed to meet the food demand of a larger global
364 population (Lamarque *et al.*, 2011; Riahi *et al.*, 2011). In contrast, 70% of P emissions from fossil fuels and
365 biofuel were expected to be removed, due to a high penetration rate of clean technology in the industrial
366 and residential sectors under both the RCP4.5 and RCP8.5 scenarios, leading to a slight difference between
367 the two scenarios.

368 3.2. Spatial distributions of N and P deposition

369 The pre-industrial (1850) and present (1997-2013) spatial distributions of N and P deposition are shown in
370 **Figure 2**. Dentener *et al.* (2006) recommended $1000 \text{ mg N m}^{-2} \text{ yr}^{-1}$ as a “critical load” threshold for plant
371 sustainability, and rates above this threshold may lead to changes in ecosystemic functioning. The
372 deposition rate of N for 1997-2013 also exceeded $1000 \text{ mg N m}^{-2} \text{ yr}^{-1}$ in large areas of India (72%), China
373 (45%) and Europe (26%). The deposition rate of P for 1997-2013 exceeded $100 \text{ mg P m}^{-2} \text{ yr}^{-1}$ in the
374 Indo-Gangetic region of India due to a high use of biofuels (*e.g.*, dung cake is widely used for cooking) and
375 in the Congo Basin in Central Africa due to deforestation (Chen *et al.*, 2010).



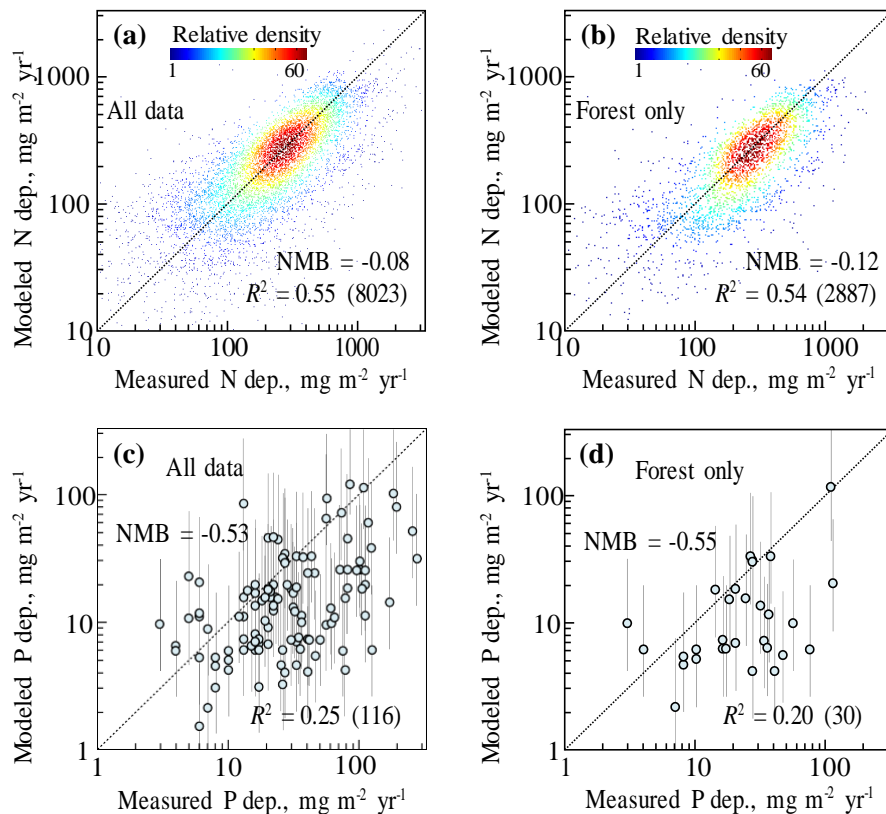
376

377

378 **Figure 2.** (a,b) Spatial distribution of N deposition in 1850 (a) and 1997-2013 (b). (c,d) Spatial distribution
379 of P deposition in 1850 (c) and 1997-2013 (d).

380

381 The modeled spatial distributions of N wet and P total deposition rates were evaluated by measurements at
382 the forest sites and at all sites (Figure 3). The comparison indicated that our model broadly captured the
383 spatial patterns in the observed deposition rates of N and P. A normalized mean bias (difference between
384 the geometric mean of the model minus the geometric mean of the measurements relative to the latter) was
385 used to quantify the bias. A statistical analysis show that 50% of the data were subject to a bias of -25% to
386 50% in the modeled wet N deposition and -4% to 164% in the modeled total P deposition relative to
387 observations (Figure S2). We addressed the potential uncertainty by scaling the modeled N deposition rate
388 by a fixed factor that followed a normal distribution, with a mean of 1.2 and a standard deviation of 0.6,
389 and the modeled P deposition by a fixed factor that followed a normal distribution, with a mean of 1.6 and
390 a standard deviation of 1.0, which were derived from the frequency distribution of the model bias (Figure
391 S2). The scaled deposition rates of N and P were used in the calculation of $\Delta C_{v,dep}$. The data for observed
392 N wet deposition enabled us to further evaluate the modeled wet deposition of N in the oxidized (NO_3) and
393 reduced (NH_4) forms by region (Figure S3).



394

395 **Figure 3.** Comparison of modelled and observed deposition of wet N (a,b) and total P (c,d). (a,c) show all
396 data and (b,d) show measurements over forests only. In (a,b), colours show the relative density of data. In
397 (c,d), the error bars show the uncertainty associated with emissions of P from different sources as estimated
398 by Wang *et al.* (2015a). Coefficient of correlation (R^2) and normalized mean bias (NMB) of log-transferred
399 deposition rates are given in each panel with the number of data in bracket.

400

401 **Figure S4** shows a comparison of our modeled surface concentrations of P for particles of the same size

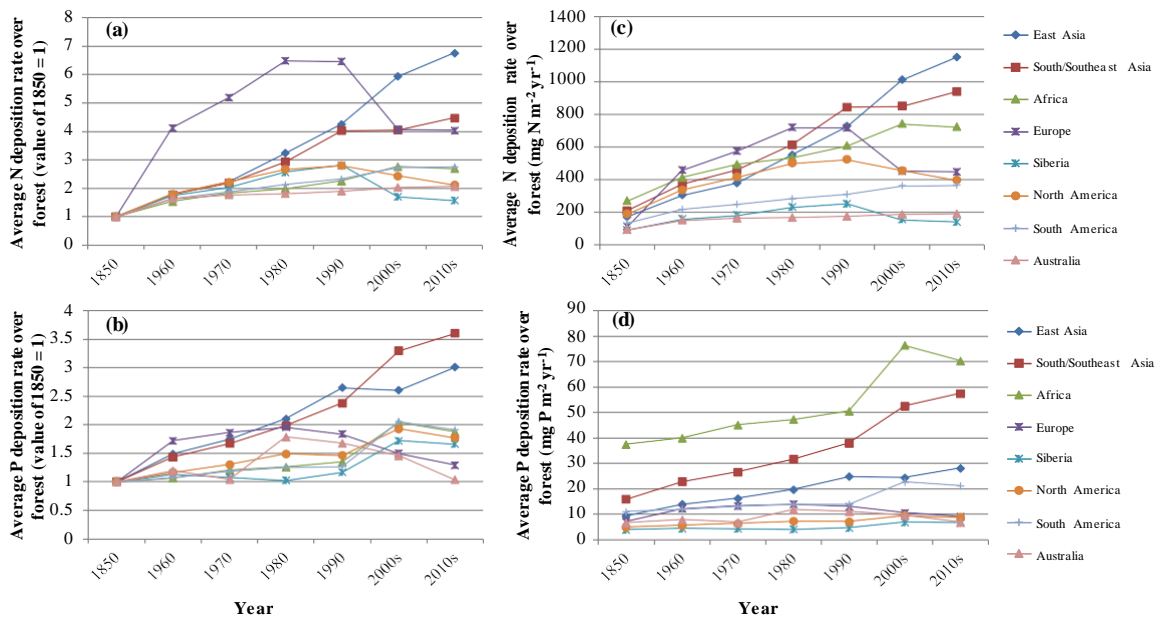
402 with the observational data used by Mahowald *et al.* (2008). These discrete sampling measurements were
403 temporally variable, so we focused on comparing the modeled P concentrations with long-term
404 measurements. It shows that including a large contribution of P from combustion sources can reduce the
405 normalized mean bias from -31% to -11%, while our estimates were subject to uncertainty errors between
406 -73% to 105% as 95% CIs in the estimation of P emissions from different sources (Wang *et al.*, 2015a).

407

408 3.3. Temporal trends of N and P deposition in forests

409 **Figure 4** shows the temporal trends of N and P deposition in forests in various regions from 1850 to the
410 present. The increase in the rate of N deposition in forests from 1850 to the present ranged from 1.5- to
411 7-fold by region. The rate of P deposition in forests increased by 1- to 3.5-fold from 1850 to the present,
412 due to a smaller contribution of anthropogenic source than for N. The deposition of N and P in North
413 American and European forests both peaked in the 1980s or 1990s. Specifically, the deposition rates of N
414 and P in European forests peaked in the 1980s and 1990s, respectively. The rate of N deposition in North
415 American forests peaked in 1990, but the rate of P deposition continued to increase. The increase in the
416 deposition of P in North American forests was mainly due to an increase in emissions from biomass
417 burning during the last two decades (Westerling, *et al.* 2006). This increase was captured by the GFED4.1
418 and ACCMIP inventories (Lamarque *et al.*, 2010; Giglio *et al.*, 2013) used in our study. **Figure S5** shows
419 that this increasing trend was also confirmed by three other inventories for biomass burning. The rate of N
420 deposition in Siberian forests had a trend similar to that of European forests due to the atmospheric
421 transport of N from Europe, but the rate of P deposition was mainly governed by the variability of wildfires.
422 The rate of N deposition in the forests in Australia and New Zealand increased continuously, but the rate of
423 P deposition began to decline in Australia after 1980 due to the replacement of P-rich fuels (coal) with
424 P-poor fuels (petroleum or natural gas) (IEA, 2013).

425 The rate of N deposition in East Asian forests was 7-fold higher in 2010 than 1850 and more than 4-fold in
426 Southern/Southeastern forests. Total N emissions were highest in China and India, but NO_x emissions had
427 increased more in China from 1990 to 2010 by 150%, compared to 80% in India, due to a faster growth in
428 fleet vehicle in China (Granier *et al.*, 2011).



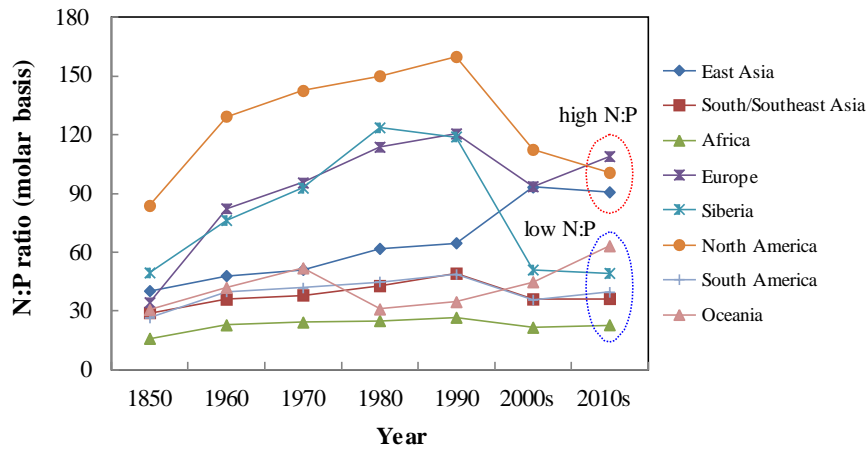
429

430 **Figure 4.** Temporal trends of N (a,c) and P (b,d) deposition rate over forests by region. (a,b) show the
 431 values relative to 1850, while (c,d) show absolute values. The data for 2000s represent an average over
 432 1997-2004 and the data for 2010s represent an average over 2005-2013.

433

434 The rate of P deposition in East Asian forests increased 2.5-fold from 1850 to 1990 and stabilized after
 435 1990. **Figure S6** shows the inter-annual variability of N- and P-deposition rates in the forests in East Asia
 436 and South/Southeast Asia from 1997 to 2013. The rate of N deposition increased continuously, but the rate
 437 of P deposition remained more stable in these two regions. The increase in the rate of N deposition was
 438 driven by the increase of in the use of fossil fuels and in agricultural activities. The rate of P deposition,
 439 however, was driven by emissions from fossil fuels, biofuel and biomass burning. The increase in fires and
 440 biomass burnt during the 1997-1998 El Niño led to a peak in the P-deposition rate in the forests in East
 441 Asia and South/Southeast Asia ([van der Werf *et al.*, 2004](#)).

442 **Figure 5** shows the temporal trends of the N:P deposition ratio (on a molar basis) in forests by region. The
 443 ratio peaked in around 1990 in the forests in Europe, Siberia and North America and then decreased due to
 444 a decline in the deposition of N and an increase in the deposition of P due to increasing wildfires. The N:P
 445 deposition ratio in the forests did not vary greatly in the forests in South/Southeast Asia, Africa and South
 446 America, because the rates of N and P deposition increased at similar rate. In contrast, the N:P deposition
 447 ratio increased continuously in the forests in East Asia due to rapid increases in the emission and deposition
 448 of N in this region. The N:P deposition ratio in the 2010s was significantly larger in the forests in Europe,
 449 North America and East Asia than in the other regions.

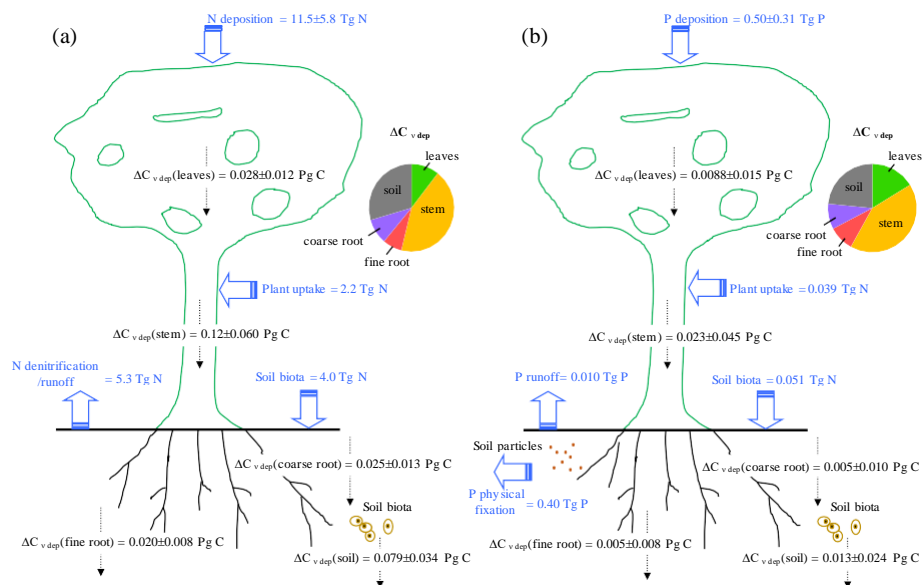


450
 451 **Figure 5.** Temporal evolution of N:P ratio in the deposition over forests by region. The data for 2000s
 452 represent an average over 1997-2004 and the data for 2010s represent an average over 2005-2013.

453

454 3.4. Forest C fixation due to anthropogenic N and P deposition

455 Based on the maps of N and P deposition, we calculated the global forest $\Delta C_{v,dep}$ using the stoichiometric
 456 mass balance approach. **Figure 6** shows that, for control values of the parameters, anthropogenic deposition
 457 of N and P for 1997-2013 led to global $\Delta C_{v,dep}$ (median \pm 90% CI from Monte Carlo simulations) of $0.27 \pm$
 458 0.13 and 0.054 ± 0.10 Pg C yr⁻¹, respectively. A total of 10 000 Monte Carlo simulations were run by
 459 randomly entering parameters from a prior uniform or normal distribution of parameters. The frequency
 460 distributions of global $\Delta C_{v,dep}$ by anthropogenic N and P deposition averaged for 1997-2013 are shown in
 461 **Figure S7**. Some parameters were uniformly or normally distributed, but the output was nearly normally
 462 distributed for $\Delta C_{N,dep}$ ($P > 0.1$) and log-normally distributed for $\Delta C_{P,dep}$ ($P > 0.2$). For a global terrestrial C
 463 sink of 3.1 ± 0.9 Pg C yr⁻¹ averaged for 2006-2015 ([Le Quere et al., 2016](#)), $\Delta C_{v,dep}$ by anthropogenic N and
 464 P deposition contributed 8.7% and 1.7% to the terrestrial C sink, respectively.



465
 466 **Figure 6.** Anthropogenic N and P deposition over forest and $\Delta C_{v,dep}$ due to anthropogenic N and P
 467 deposition per year as an average over 1997-2013. (a) for N and (b) for P. Uncertainty of the modeled N

468 and P deposition as standard deviations is derived from a comparison with observations. Uncertainty of the
 469 $\Delta C_{v\text{ dep}}$ as 90% CI is derived from Monte Carlo simulations. The pie charts show the distribution of $\Delta C_{v\text{ dep}}$
 470 among five pools.

471

472 **Figure 6** also shows that 43% of $\Delta C_{N\text{ dep}}$ was stored in stems, followed by soil (29%), leaves (11%), coarse
 473 roots (9%) and fine roots (7%). Similarly, stems (42%) were the most important storage pool for $\Delta C_{P\text{ dep}}$. In
 474 addition, we performed sensitivity tests using the lower or upper bounds of the parameters to investigate the
 475 influences on our estimated $\Delta C_{N\text{ dep}}$ (**Table 2**). It shows that the major parameters influencing $\Delta C_{v\text{ dep}}$ by N
 476 or P include the retention ratios of N in vegetation and soils, the physical fixation of P by soil, the fraction
 477 of N and P allocated to woody biomass, and the C:N and C:P stoichiometric ratios in each pool. $\Delta C_{P\text{ dep}}$ was
 478 generally associated with a far higher uncertainty than $\Delta C_{N\text{ dep}}$. Most importantly, we assumed that a large
 479 fraction of P (80%) was fixed by the soil as inorganic P, which is unavailable for C storage ([Walker and](#)
 480 [Syres, 1976](#)). Assuming a weaker or stronger fixation of P by soils, which influences estimates of $\Delta C_{v\text{ dep}}$
 481 by P the most, however, led to a difference in $\Delta C_{P\text{ dep}}$ from -70% to +300%.

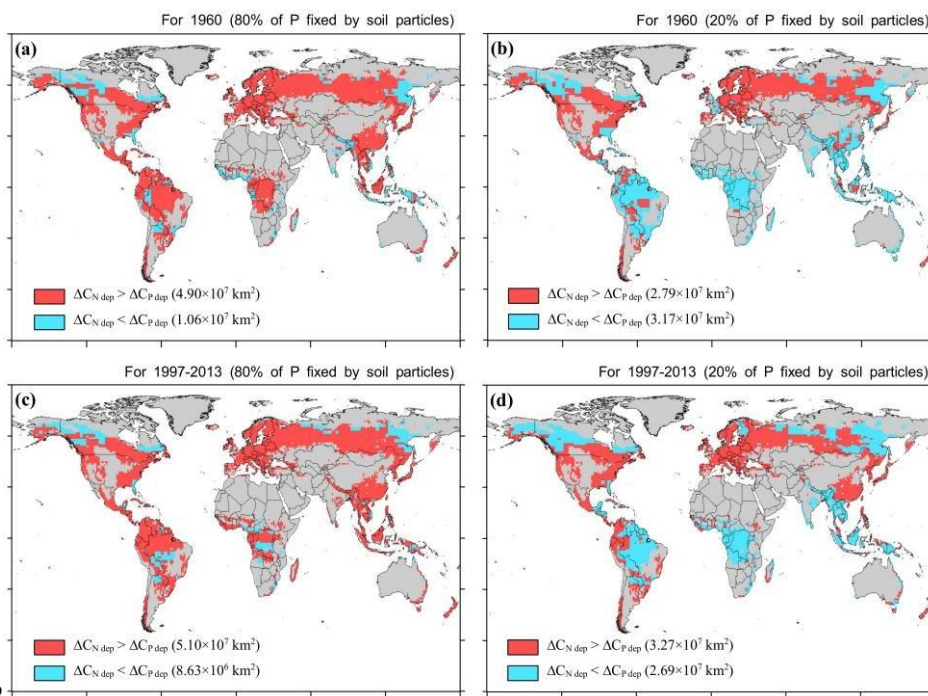
482 **Table 2. Global forest $\Delta C_{v\text{ dep}}$ due to anthropogenic N and P deposition over 1997-2013.** Sensitivity
 483 tests were run to compare with a standard run with central values of parameter. The sensitivity tests include
 484 high or low retention fraction of N in vegetation and soil; weak or strong fixation of P by soil particles;
 485 high or low fraction of N and P allocated to the woody part; high or low C:N and C:P stoichiometric ratios.
 486 Values in brackets show the percentage changes relative to the standard run.

	Leaf	Stem	Fine root	Coarse root	Soil	Woody	Total
Forest $\Delta C_{v\text{ dep}}$ by N deposition over 1997-2013 (Pg C yr⁻¹)							
Standard run	0.028	0.117	0.020	0.025	0.079	0.142	0.269
High retention fraction	0.037	0.153	0.026	0.033	0.107	0.186 (+31%)	0.356 (+32%)
Low retention fraction	0.018	0.073	0.013	0.016	0.042	0.088 (-38%)	0.160 (-40%)
High woody fraction	0.021	0.168	0.014	0.037	0.079	0.205 (+45%)	0.320 (+19%)
Low woody fraction	0.034	0.079	0.022	0.017	0.079	0.097 (-32%)	0.232 (-14%)
High C:N ratio	0.034	0.140	0.024	0.030	0.079	0.170 (+20%)	0.307 (+15%)
Low C:N ratio	0.023	0.093	0.016	0.020	0.079	0.113 (-20%)	0.231 (-15%)
Forest $\Delta C_{v\text{ dep}}$ by P deposition over 1997-2013 (Pg C yr⁻¹)							
Standard run	0.009	0.023	0.005	0.005	0.013	0.028	0.054
Weak fixation by soil	0.035	0.091	0.020	0.020	0.051	0.111 (+300%)	0.218 (+300%)
Strong fixation by soil	0.003	0.007	0.002	0.002	0.004	0.008 (-70%)	0.016 (-70%)
High woody fraction	0.006	0.039	0.003	0.009	0.013	0.048 (+73%)	0.070 (+29%)
Low woody fraction	0.009	0.018	0.005	0.004	0.013	0.022 (-19%)	0.050 (-8%)
High C:P ratio	0.011	0.027	0.006	0.006	0.013	0.033 (+20%)	0.063 (+15%)
Low C:P ratio	0.007	0.018	0.004	0.004	0.013	0.022 (-20%)	0.046 (-15%)

487

488 3.5. Spatial patterns of N and P limitation

489 Increasing N from atmospheric deposition has been postulated to lead to a progressive emerging limitation
 490 of P (Vitousek *et al.*, 1984, 2010; Penuelas *et al.*, 2013). **Figure 7** compares the forest area where $\Delta C_{N\text{ dep}}$ is
 491 larger than $\Delta C_{P\text{ dep}}$ between 1960 and the present (1997-2013) under different assumptions of the physical
 492 fixation of P by the soil. A faster increase in the deposition of N than P in forests close to industrialized
 493 regions had led to a growth in $\Delta C_{v\text{ dep}}$ that is higher for N than for P. It should be noted that, as we did not
 494 account for other sources of N and P (*e.g.* weathering for P and nitrification for N), lower $\Delta C_{v\text{ dep}}$ from N
 495 than P deposition is only one factor contributing to a limitation by P (Vitousek *et al.*, 1984, 2010; Penuelas
 496 *et al.*, 2012, 2013). Globally, the forests where $\Delta C_{N\text{ dep}}$ is larger than $\Delta C_{P\text{ dep}}$ in 1960 covered an area
 497 between 2.79 and 4.90×10^7 km², depending on the strength of soil P fixation. In these forests, additional
 498 supply of P from other sources (*e.g.*, by mineralization) is needed to support $\Delta C_{v\text{ dep}}$ by N. The forest area
 499 where $\Delta C_{N\text{ dep}}$ is larger than $\Delta C_{P\text{ dep}}$ had extended by 4% or 18% from 1960 to the present, which also
 500 depends on the strength of soil P fixation, mainly located in forests in South/Southeast Asia, East Asia,
 501 Europe and North America.



502 **Figure 7.** Spatial distribution of forest area where $\Delta C_{v\text{ dep}}$ by anthropogenic N deposition is larger or
 503 smaller than $\Delta C_{v\text{ dep}}$ by anthropogenic P deposition in 1960 (**a,b**) and as an average over 1997-2013 (**c,d**).
 504 In (**a,c**), the model assumes that 80% of the deposited P is fixed by soil particles, while (**b,d**) shows results
 505 in a sensitivity case where 20% of P is fixed by soil particles. The total areas where $\Delta C_{v\text{ dep}}$ by
 506 anthropogenic N deposition is larger or smaller than $\Delta C_{v\text{ dep}}$ by anthropogenic P deposition are in
 507 parentheses. Non-forest land areas are shown as grey.

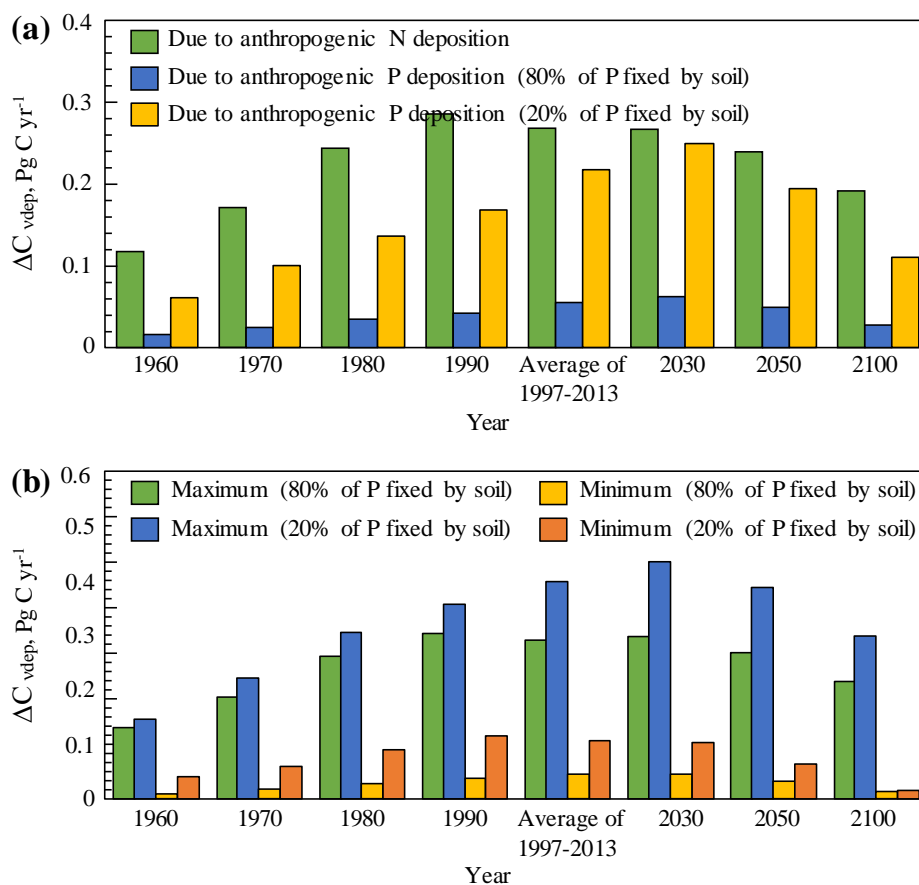
508

510 3.6. Temporal trends of $\Delta C_{v\text{ dep}}$ by N and P

511 **Figure 8a** shows the temporal trends of $\Delta C_{v\text{ dep}}$ by N and P deposition alone for 1960-2100 under different
 512 physical fraction of P fixed in soil. $\Delta C_{v\text{ dep}}$ by N peaked in 1990 and then declined due to reductions of N
 513 emissions and deposition in the forests in Europe and North America, but $\Delta C_{v\text{ dep}}$ by P was projected to

514 increase by 2030 due to continuous increases in P emissions and deposition in South and Southeast Asia,
 515 Africa and South America under the RCP4.5 scenario. We also found that $\Delta C_{v\text{dep}}$ by N was much higher
 516 than $\Delta C_{v\text{dep}}$ by P in our central case where 80% of the P was fixed by soil, but they were very similar in a
 517 sensitivity test where only 20% of P was fixed by soil. $\Delta C_{v\text{dep}}$ by N for 2030, 2050 and 2100 was expected
 518 to be 28-60% higher under the RCP8.5 than the RCP4.5 scenario due to higher NH_3 emissions from
 519 agriculture. Difference in $\Delta C_{v\text{dep}}$ by P would be less than 15% due to a high control rate of industrial
 520 particulate emissions under both scenarios (Lamarque *et al.*, 2011) (Figure S8).

521 Based on $\Delta C_{v\text{dep}}$ by N and P in each $1^\circ \times 1^\circ$ grid, we calculated $\Delta C_{v\text{dep}}$ by N and P deposition together in
 522 the case of maximum or minimum effects from 1960 to 2100 (Figure 8b). $\Delta C_{v\text{dep}}$ was about 6-fold higher
 523 for maximum (0.28 Pg C yr^{-1} averaged for 1997-2013) than minimum (0.044 Pg C yr^{-1}) effects,
 524 highlighting the imbalance between N and P in the deposition. $\Delta C_{v\text{dep}}$ for maximum effects peaked at 0.29
 525 Pg C yr^{-1} in 1990 and then decreased due to reductions of N emissions and deposition rates in the forests in
 526 Europe and North America. In a sensitivity test where 20% of P was fixed by soil, however, $\Delta C_{v\text{dep}}$ for
 527 maximum effect was predicted to increase continuously from 0.14 Pg C yr^{-1} in 1960 to 0.42 Pg C yr^{-1} in
 528 2030 due to increases in both N and P deposition rates before 1990 and an increase in P deposition rate
 529 alone after 1990. Figure S8 shows $\Delta C_{v\text{dep}}$ due to N and P together under the RCP8.5 scenario, where $\Delta C_{v\text{dep}}$
 530 for maximum effect was expected to be 23-54% higher than under the RCP4.5 scenario.



531

532

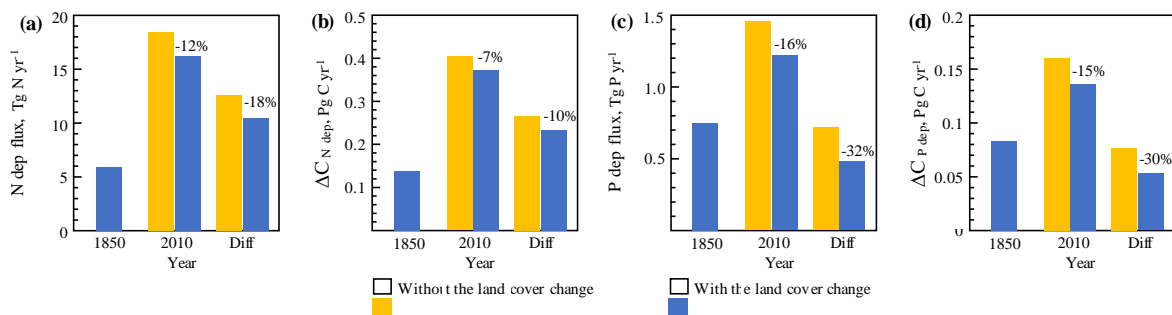
533 **Figure 8.** Temporal trends of global $\Delta C_{v\text{dep}}$ due to anthropogenic N and P deposition alone (a) and together
 534 as maximum or minimum effects (b) from 1960 to 2100. $\Delta C_{v\text{dep}}$ in a case where 80% of P is fixed by soil

535 is compared to a sensitivity case where 20% of P is fixed by soil. The $\Delta C_{v\text{ dep}}$ for 2030, 2050 and 2100 are
 536 estimated based on the anthropogenic N and P deposition under the RCP 4.5 storyline.

537

538 3.7. Impact of forest cover change on $\Delta C_{v\text{ dep}}$

539 In addition to the change of N and P deposition rates, the change of forest areas due to deforestation and
 540 afforestation influences $\Delta C_{v\text{ dep}}$. **Table S4** shows the change of total forest areas, average N and P
 541 deposition fluxes over forests and $\Delta C_{v\text{ dep}}$ estimated for the five types of forests using a reconstructed
 542 global data set of forest cover change from 1850 to 2010 (Peng *et al.*, 2017). **Figure 9** compares the
 543 deposition fluxes and the $\Delta C_{v\text{ dep}}$ for 1850 and 2010 with or without forest cover change by taking 1850 as
 544 a reference, whereas the results for 2010 are calculated using the forest cover map in 1850 or 2010. It
 545 shows that, if accounting for forest cover change, $\Delta C_{v\text{ dep}}$ due to change in N and P deposition from 1850 to
 546 2010 would decrease by 10% and 30%, respectively. Likewise, the deposition fluxes and $\Delta C_{v\text{ dep}}$ for 1850
 547 and 2010 are compared with or without the forest cover change by taking 2010 as a reference, whereas the
 548 results for 1850 are calculated using the forest cover map in 1850 or 2010 (**Figure S9**). Similarly, it shows
 549 that the forest cover change leads to a difference in $\Delta C_{v\text{ dep}}$ by -6% and -19% for N and P, respectively.



550

551 **Figure 9.** Comparison of global N deposition fluxes over forests (a), $\Delta C_{v\text{ dep}}$ due to N deposition (b), P
 552 deposition fluxes over forests (c) and $\Delta C_{v\text{ dep}}$ due to P deposition (d) in 1850 and 2010 and the difference
 553 between 1850 and 2010 (Diff) without or with the forest cover change by taking year 1850 as a reference.
 554 The yellow bars show the $\Delta C_{v\text{ dep}}$ calculated based on the forest cover map in 1850, and the blue bars show
 555 the $\Delta C_{v\text{ dep}}$ calculated based on the forest cover map for 1850 and 2010 respectively. In all cases, $\Delta C_{v\text{ dep}}$ is
 556 estimated using the central values of parameters. Relative difference as a percentage by accounting for the
 557 forest cover change is given over each bar.

558

559 There are three reasons for the difference. First, the global total forest area had declined by 12% from 29.5
 560 $\times 10^6$ km² in 1850 to 25.9×10^6 km² in 2010. Second, the C response to N or P deposition varies across the
 561 five types of forest and change in the relative cover of each forest type influences the estimation of $\Delta C_{v\text{ dep}}$.
 562 For example, the C response to N deposition is the highest for the evergreen needle-leaf forests (47 kg C kg
 563 N⁻¹) and the lowest for the evergreen broadleaf forests (12 kg C kg N⁻¹). From 1850 to 2010, the cover
 564 fraction of evergreen needle-leaf forests had increased from 19% to 21%, while the cover of evergreen
 565 broadleaf forests had decreased from 49% to 44%, leading to less reduction in $\Delta C_{N\text{ dep}}$ than N deposition
 566 fluxes after accounting for the land cover change (**Figure 9**). At last, change in the spatial distribution of
 567 forests also leads to some changes in the average N or P deposition rates, but our data sets show that this
 568 influence is relatively small. The average N and P deposition rates over global forests in 2010 were 628 mg

569 N m⁻² yr⁻¹ and 47 mg P m⁻² yr⁻¹ using the forest cover map in 2010, compared with 626 mg N m⁻² yr⁻¹ and
570 49 mg P m⁻² yr⁻¹ using the forest cover map in 1850.

571

572 4. Discussion

573 4.1. Global data sets of N and P deposition

574 Our study provides the first global gridded data sets for both N and P deposition from pre-industrial (1850),
575 historical periods (1960, 1970, 1980 and 1990), to present (1997-2013), and into the future (2030, 2050 and
576 2100) from a global climate-chemistry model driven by complete bottom-up emission inventories. **Table**
577 **S1** provides a comparison of species represented by the model, horizontal resolution, and observational
578 data used to evaluate the model with previous studies. In the simulation of N, we employed state-of-the-art
579 inventories for reactive N and other tracers that influence the atmospheric chemistry of N (Klimont *et al.*,
580 2013). The chemistry of N in the model is advanced in the treatments of the ammonia cycle and the nitrate
581 particle formation (Hauglustaine *et al.*, 2014), which are only represented in few global models (Dentener
582 *et al.*, 2006). Our model also provides a horizontal resolution of 1.2°×2.5° that is finer than most of
583 previous models (Dentener *et al.*, 2006). For P, we used a new emission inventory from combustion
584 sources with the uncertainties quantified (Wang *et al.*, 2015a), which reduced the underestimation in the
585 modeled P deposition by covering P in all sizes of particles which are carried to the measurement sites.
586 Prior to our work, there was only one global data set of present day P deposition available (Mahowald *et al.*,
587 2008). In addition to its lack of temporal changes, this previous data set covered P in particles with
588 diameter smaller than 10 μm. Wang *et al.* (2015a) showed that it led to a discrepancy between the modeled
589 and observed P deposition rates at globally distributed measurement stations if P in particles with diameter
590 larger than 10 μm was neglected even if uncertainties in P emissions from other sources were accounted
591 for.

592 The modeled NO₃ and NH₄ wet deposition rates were evaluated by comparing with 8023 observations from
593 globally distributed measurement stations. The modeled P deposition rates were compared with 116
594 observations. The normalized mean bias (NMB) is -8% for the NO₃ and NH₄ wet deposition rates, and
595 -53% for the P deposition rates. It also shows that 50% of the data were associated with a bias between
596 -25% and 50% for the NO₃ and NH₄ wet deposition and between -4% and 164% for the P deposition. The
597 correlation coefficient of the log-transformed deposition rate is higher for N ($R=0.74$) than for P ($R=0.50$).
598 The underestimation of P deposition was likely due to errors in the transport model or ignored local
599 biogenic aerosols in the measurement samples. The distributions of these model errors were treated as
600 uncertainties in our data sets. It is not a surprise that there is a larger uncertainty associated with the
601 modeled deposition rates of P than N. For P, in addition to the errors associated with atmospheric transport
602 and removal, emissions of P from wind erosion of soil dusts, biogenic aerosols, marine sea-salt particles,
603 volcanoes and other sources (*e.g.*, phosphine from freshwater wetlands and rice paddies) are all subject to
604 high uncertainties (Graham and Duce, 1979; Mahowald *et al.*, 2008; Wang *et al.*, 2015a). A limitation of
605 our P deposition simulations set is that the long-term variations of these emissions are not resolved, because

606 no information on evolution of these sources is currently available at the global scale. More measurements
607 of P deposition rates in contrasting environments are useful to reduce the uncertainty in the modeled P
608 deposition rates (e.g., [Du et al., 2016](#)), while more long-term measurements of the surface concentrations of
609 P with additional source information are useful to constrain the model and emissions of P from difference
610 sources ([Mahowald et al., 2008](#)).

611 For N, we had lower model biases in some regions when compared with previous studies. For example,
612 [Hauglustaine et al. \(2014\)](#) simulated N deposition using the same climate-chemistry model and evaluated
613 the model using 4036 observations from global monitoring stations. They reported that NMB is
614 respectively -32%, -4.5% and -60% in North America, Europe and Asia for the modeled NH₄ wet
615 deposition, and -28%, 13% and -54% for the modeled NO₃ wet deposition. In contrast, NMB in our study is
616 -12% in North America, -42% in Europe and -28% in East Asia respectively for NH₄ wet deposition, and
617 29%, -29% and -11% respectively for NO₃ wet deposition (**Figure S3**). Thus, our results are better for Asia
618 but worse for Europe. [Hauglustaine et al. \(2014\)](#) attributed the underestimation in Asia to a coarse
619 horizontal resolution of the model and an underestimation of reactive-N emissions in the region ([Lamarque](#)
620 [et al., 2010](#)). We updated reactive-N emissions by using a more recent ECLIPSE GAINS.4a inventory
621 ([Klimont et al., 2013](#)) and used a higher horizontal resolution version of the atmospheric model, from
622 1.9°×3.75° previously to 1.2°×2.5°. These together reduced the model bias in Asia. Despite a larger NMB
623 in Europe in our model, the correlation coefficient (*R*) is 0.63 and 0.79 for wet NH₄ and NO₃ deposition in
624 this region, respectively, higher than 0.33 and 0.49 by [Hauglustaine et al. \(2014\)](#), indicating that our model
625 better captures the spatial pattern of N deposition.

626 Overall, our study provides consistent gridded simulations of both N and P deposition at a high horizontal
627 resolution, which agrees better with observations from a large number of globally distributed measurement
628 stations than previous studies ([Mahowald et al., 2008](#); [Hauglustaine et al., 2014](#)). A statistical analysis of
629 the model-observation comparison generates a probabilistic distribution of the model bias, which enabled
630 us to address the uncertainty in our data sets. Whereas previous studies ([de Vries et al., 2014](#)) have only
631 estimated the C sequestration by current N deposition without spatial and temporal variations, we estimated
632 C sink changes from changes in N and P deposition maps and included an uncertainty analysis to both N, P
633 deposition and C sink responses.

634 **4.2. P deposition contributes significantly to forest C storage**

635 Increasing atmospheric CO₂ concentrations, longer growing season and N fertilization have been suggested
636 to lead to limitation by P of productivity in temperate forests ([Vitousek et al., 1984, 2010](#); [Penuelas et al.,](#)
637 [2012, 2013](#)). Our long-term data of P-deposition rates, combined with data of N-deposition rates, suggested
638 that $\Delta C_{P\text{ dep}}$ would be close to $\Delta C_{N\text{ dep}}$ if 20% of the P is fixed by soil, and C fixation due to P deposition is
639 higher than previously estimated ([Cleveland et al., 2013](#); [de Vries et al., 2014](#)) due to higher P deposition
640 rates and a less fraction of P loss ([Sattari et al., 2012](#)). Our simple stoichiometric mass balance approach
641 indicated that the strength of P fixation by soil particles exerted the strongest influence on the response of C
642 fixation to P deposition. Consequently, we adopted a global-constant fraction of deposited P being fixed by

643 soil ranging from 20% to 94%, based on the transfer coefficients between stable and labile P from Sattari *et*
644 *al.* (2012). However, it should be noted that this fraction was not uniform in space and was probably soil
645 type dependent (Compton and Cole, 1998). More field experiments measuring fixation of P by soil particles
646 are needed to reduce this uncertainty (Johnson *et al.*, 2003).

647 Nevertheless, our stoichiometric method found that $\Delta C_{P\ dep}$ was equivalent to 50-90% of $\Delta C_{N\ dep}$ when the
648 fixation of P by soil was weak, implying that deposited P can contribute to forest C storage providing that
649 other sources of N and P were held constant. Spatially, $\Delta C_{P\ dep}$ could even exceed $\Delta C_{N\ dep}$ in some areas of
650 forests in East Asia, South and Southeast Asia, Africa and South America (Figure 7). In particular, we find
651 that $\Delta C_{P\ dep}$ can be significantly higher than $\Delta C_{N\ dep}$ in tropical forests in the Congo and Amazon Basins and
652 Indonesia, due to both rapid losses of N from ecosystems through denitrification (Bai *et al.*, 2012) and high
653 deposition rates of P from deforestation fire emissions (Giglio *et al.*, 2013). The C sink in tropical forests is
654 sensitive to additional P inputs, because P availability in the soil of tropical forests was found to be far
655 lower than the global average (Yang *et al.*, 2013) but P use efficiency was higher than that in boreal forests
656 (Gill and Finzi, 2016). We suggest that more attentions should be paid to estimate the C sink due to
657 additional P inputs from deposition in tropical forests.

658 However, our current knowledge of nutrient cycling is more limited for P than for N, leading to high
659 uncertainties global ecosystem-level models (Wang *et al.*, 2010; Goll *et al.*, 2012; Yang *et al.*, 2014). It is
660 known that most of P is neither directly taken up by plant nor lost by leaching, but a large fraction of P is
661 fixed by soils before being slowly transferred into a labile pool that can be used by plant (Aerts and Chapin,
662 2000; Sattari *et al.*, 2012). Different from N, there is no atmospheric loss pathway for P, while P is less
663 mobile in soil and hence less prone to leaching than for N (Aerts and Chapin, 2000; Goll *et al.*, 2012; Goll,
664 2016), but it remains unknown whether and how fast the fixed P in soil can be mineralized and used by
665 plants (Lü *et al.*, 2013). A meta-analysis of P and N plus P fertilization experiments suggested that
666 increasing N availability, *e.g.* from increasing N deposition, tends to increase P cycling rate and thus
667 contributes to use of P by plants (Marklein and Houlton, 2012). Measurements of the rate of P uptake in the
668 seasons with both high N and P-deposition rates are useful to understand the contribution of N and P
669 deposition together to the C fixation in forests.

670 The cycles of C, N and P differ in their respect to the residence time in terrestrial ecosystem (Walker and
671 Syres, 1976). Our stoichiometric method attributes the C storage due to N and P deposition at a timescale
672 of 10-20 years, following de Vries *et al.* (2014). Nonetheless, P would turn over much more slowly than N
673 (Walker and Syres, 1976), so it is worth highlighting that the effects of P would last longer than those of N.
674 We expect that the use by plants is much slower for deposited P than deposited N due to the strong physical
675 fixation of P in soil (Aerts and Chapin, 2000; Goodale *et al.*, 2002), and our estimated $\Delta C_{P\ dep}$ under a weak
676 fixation should include part of the long-term effects of P deposition. Under a high CO₂ concentration in the
677 near term, plants are likely increasing their efficiency in accessing and utilizing these not readily available
678 P (Buendia *et al.*, 2014, Goll, 2016). Such effects should be better represented in the process-based models
679 when studying the impact of N and P deposition on P limitation (Cleveland *et al.*, 2013; Wieder *et al.*,

680 2015).

681 While we cannot quantify all sources of N and P for plants, calculation of maximum and minimum $\Delta C_{v\text{ dep}}$
682 by N and P provides a preliminary estimation of the C storage supported by anthropogenic P deposition.
683 Under a weak fixation for P by soil, maximum $\Delta C_{v\text{ dep}}$ by N and P ($0.38 \text{ Pg C yr}^{-1}$) is 43% higher than $\Delta C_{v\text{ dep}}$
684 by N alone ($0.27 \text{ Pg C yr}^{-1}$). Meanwhile, minimum $\Delta C_{v\text{ dep}}$ by N and P ($0.10 \text{ Pg C yr}^{-1}$) is 53% lower
685 than $\Delta C_{v\text{ dep}}$ by P alone ($0.22 \text{ Pg C yr}^{-1}$). They both suggest a potential contribution of anthropogenic P
686 deposition to additional forest C sink. The map of $\Delta C_{v\text{ dep}}$ by N and P also implies that other sources of N
687 are needed to support the C storage by P deposition in some Asian tropical forests where the deposition rate
688 increased faster for P than for N (Figure 7). However, it should be noted that N fertilization can also exert a
689 significant effect on the capacity of plant to use the P (Marklein and Houlton, 2012; Lü *et al.*, 2013), and
690 the maximal co-fertilized $\Delta C_{v\text{ dep}}$ is likely even larger than maximum $\Delta C_{v\text{ dep}}$ estimated by our method.

691 4.3. Uncertainty due to N retention by the canopy

692 We aimed at providing a preliminary estimation of forest C response to N and P deposition and investigated
693 the imbalance of N and P in the deposition at a mid-term scale of 10-20 years when other sources were held
694 constant. We find that anthropogenic P deposition can contribute to C storage, supplementing $\Delta C_{v\text{ dep}}$
695 supported by anthropogenic N deposition by 43%. It is worth highlighting that the impact of N deposition
696 on C storage also remains uncertain, despite more measurements of N than P retention in ecosystems, due
697 largely to the uncertain impact of canopy N uptake. It was noticed that ~40% of N deposited is retained by
698 the canopy in Europe and North America (Lovett and Lindberg, 1993), but the impact on C storage is not
699 well constrained (Sparks, 2009). Sievering *et al.* (2007) found that 80% of the growing-season N deposition
700 was retained in canopy foliage and branches and that ~20% of daytime net ecosystem exchange may be
701 attributed to canopy N uptake. Dezi *et al.* (2010) found that the net ecosystem production would be
702 increased by 58% under a hypothesis that canopy N uptake can directly stimulate photosynthesis relative to
703 without canopy N uptake. Nair *et al.* (2016) suggested that accounting for canopy N uptake could lead to an
704 increased C response to N deposition (oC/oN) from 43 to $114 \text{ kg C kg N}^{-1}$ (by 2.6-fold) through a
705 well-designed mesocosm experiment. It should be noted that the experiment by Nair *et al.* studied the
706 response to N deposition at a time scale of one year and it is likely that N in the aboveground biomass can
707 be re-allocated in plants at a longer time scale. This is likely the reason why most of applied N was retained
708 in the plants at mid-long term (Gaije *et al.*, 2007), but most of the N in the plant was recovered in the bark
709 rather than in the canopy (Dail *et al.*, 2009).

710 Here we calculated the C response to N deposition based on the fate of deposited N at a timescale of 10-20
711 years following de Vries *et al.* (2014). We estimated that oC/oN was $24 \text{ kg C kg N}^{-1}$, which is lower than
712 the estimate by Nair *et al.* (2016), but close to the estimate ($11.5\text{-}39.8 \text{ kg C kg N}^{-1}$) by de Vries *et al.* (2014),
713 because Nair *et al.* (2016) did not account for loss of N in the ecosystem via denitrification and leaching.
714 We increased our estimate of $\Delta C_{N\text{ dep}}$ by 2.6-fold as indicated by Nair *et al.*'s experiment to yield an upper
715 estimate of the effect by N. Consequently, maximum $\Delta C_{v\text{ dep}}$ by N and P increased by 2-fold from 0.38 Pg
716 C yr^{-1} to $0.76 \text{ Pg C yr}^{-1}$, compared to $0.70 \text{ Pg C yr}^{-1}$ by anthropogenic N deposition, while minimum $\Delta C_{v\text{ dep}}$

717 increased by 1.6-fold from 0.10 to 0.16 Pg C yr⁻¹, compared to 0.22 Pg C yr⁻¹ by anthropogenic P
718 deposition. This suggests that the effect of P will be less significant if the high C response to N deposition
719 due to direct use of N by the canopy can be confirmed by more evidences.

720 4.4. Ecological implications of N and P deposition

721 The spatial patterns and temporal trends of N and P emissions and subsequent deposition are important for
722 understanding the variation of nutrient limitation in forests far away from agricultural activities (Reay *et al.*,
723 2008). Manipulation experiments across global biomes found that many ecosystems are co-limited by the
724 availability of N and P (Elser *et al.*, 2007; LeBauer and Treseder, 2008; Penuelas *et al.*, 2013). Fossil fuel,
725 biofuel and deforestation fires provide additional N and P to forests beyond the background level and these
726 emitted from the populated regions can reach remote forests by atmospheric transport. Our long-term data
727 of the deposition for both N and P help to quantify the deposition of N and P as anthropogenic components
728 and to estimate the additional C storage in forests.

729 Global change in N and P deposition rates arising from N and P emissions by human activities and biomass
730 burning is only one of factors that influence carbon storage by forests. Our study made a preliminary
731 attempt to assess the contributions of forest cover change (Peng *et al.*, 2017) and the changes in N and P
732 deposition rates to the $\Delta C_{v, dep}$. It is not a surprise that forest cover change has offset 10% and 30% of
733 increase in the $\Delta C_{v, dep}$ from 1850 to 2010 due to increase in N and P deposition rates, due to decline in
734 forest areas mainly in the tropics. In addition to forest cover change, other environmental drivers perturbing
735 the forest C sequestration from nutrient deposition, such as rising CO₂ levels (Field *et al.*, 1995),
736 emergency of large-scale drought (Phillips *et al.*, 2009), spring and autumn warming (Piao *et al.*, 2008) and
737 change in forest water-use efficiency (Keenan *et al.*, 2013), are not considered in this study. A combination
738 of our global N and P deposition data sets associated with their uncertainties with process-based vegetation
739 models including both N and P interactions with terrestrial C cycling (*e.g.*, Wang *et al.*, 2010; Goll *et al.*,
740 2012) would permit a more comprehensive understanding of the impact of atmospheric deposition on the
741 forest carbon sink.

742 Using a conceptual stoichiometric mass balance approach, we showed that anthropogenic N deposition for
743 1997-2013 contributed ~9% to the global terrestrial C sink, which is close to a previous estimate of 10% for
744 2030 (Reay *et al.*, 2008). We emphasized that physical P fixation is an important factor that can lead to an
745 imbalance between N and P in atmospheric deposition. Anthropogenic P deposition (0.50 Tg P yr⁻¹) was
746 23-fold lower than N deposition (11.5 Tg N yr⁻¹) for 1997-2013, but most of the P was stored in soils on a
747 shorter term and less P than N was prone to loss (5.3 Tg N yr⁻¹ was lost for N by denitrification or leaching,
748 and only 0.010 Tg P yr⁻¹ was lost for P by leaching). Our analysis suggested that historical P deposition
749 would likely exert a significant cumulative effect on the terrestrial C sink by releasing soil-fixed P in the
750 long term. Nonetheless, our stoichiometric approach cannot account for the effects of N and P deposition
751 under elevated CO₂ concentration and varying climate (Gruber and Galloway, 2008; Vitousek *et al.*, 2010).
752 Comprehensive process-based Earth System ecosystem models representing the biogeochemical cycles of
753 C, N and P are useful for understanding the ecological effects of historical, present and future depositions

754 of N and P on the C cycle (Reed *et al*, 2015).

755 **Acknowledgements**

756 The authors thank Ether/ECCAD for the distribution of emissions used in this study. This study was funded
757 by FABIO, a Marie Curie International Incoming Fellowship funded by the European Commission (Project
758 No 628735) and the IMBALANCE-P project of the European Research Council (ERC-2013-SyG-610028).
759 The simulations were performed using DSM-CCRT resources under the GENCI (Grand Equipement
760 National de Calcul Intensif) allocation of computer time (grant 2016-t2014012201).

761 **References**

- 762 Ahlström, A., Schurgers, G., Arneth, A., & Smith, B. (2012). Robustness and uncertainty in terrestrial
763 ecosystem carbon response to CMIP5 climate change projections. *Environmental Research Letters*, **7**,
764 044008.
- 765 Aerts, R., & Chapin, F. S. (2000). The mineral nutrition of wild plants revisited: a re-evaluation of
766 processes and patterns. *Advances in Ecological Research*, **30**, 1-67
- 767 Bai, E., Houlton, B. Z., & Wang, Y. P. (2012). Isotopic identification of nitrogen hotspots across natural
768 terrestrial ecosystems. *Biogeosciences*, **9**, 3287-3304.
- 769 Balkanski, Y. (2011). L'Influence des Aérosols sur le Climat, Thèse d'Habilitation à Diriger des
770 Recherches, Université de Versailles Saint-Quentin, Saint-Quentin-en-Yvelines.
- 771 Bouwman, A. F., Lee, D. S., Asman, W. A., Dentener, F. J., Van Der Hoek, K. W., & Olivier, J. G. J.
772 (1997). A global high- resolution emission inventory for ammonia. *Global Biogeochemical Cycles*, **11**,
773 561-587.
- 774 Buendía, C., Arens, S., Hickler, T., Higgins, S. I., Porada, P., & Kleidon, A. (2014). On the potential
775 vegetation feedbacks that enhance phosphorus availability-insights from a process-based model linking
776 geological and ecological timescales. *Biogeosciences*, **11**, 3661-3683.
- 777 Chen, Y., Randerson, J. T., van der Werf, G. R., Morton, D. C., Mu, M. Q., & Kasibhatla, P. S. (2010).
778 Nitrogen deposition in tropical forests from savanna and deforestation fires. *Global Change Biology*, **16**,
779 2024-2038.
- 780 Cleveland, C. C., Houlton, B. Z., Smith, W. K., Marklein, A. R., Reed, S. C., Parton, W., ..., Running, S.
781 W. (2013). Patterns of new versus recycled primary production in the terrestrial biosphere. *Proceedings of*
782 *the National Academy of Sciences*, **110**, 12733-12737.
- 783 Compton, J. E., & Cole, D. W. (1998). Phosphorus cycling and soil P fractions in Douglas-fir and red alder
784 stands. *Forest Ecology and Management*, **110**, 101-112.
- 785 Dail, D. B., Hollinger, D. Y., Davidson, E. A., Fernandez, I., Sievering, H. C., Scott, N. A., & Gaige, E.
786 (2009). Distribution of nitrogen-15 tracers applied to the canopy of a mature spruce-hemlock stand,
787 Howland, Maine, USA. *Oecologia*, **160**(3): 589-599.
- 788 de Vries, W., van der Salm, C., Reinds, G. J., & Erisman, J. W. (2007). Element fluxes through European
789 forest ecosystems and their relationships with stand and site characteristics. *Environmental Pollution*, **148**,
790 501-513.
- 791 de Vries, W., Du, E., & Butterbach-Bahl, K. (2014). Short and long-term impacts of nitrogen deposition on

792 carbon sequestration by forest ecosystems. *Current Opinion in Environmental Sustainability*, **9**, 90-104.
793 Dentener, F., Drevet, J., Lamarque, J. F., Eickhout, B., Fiore, A. M., Hauglustaine, D., ..., Wild, O. (2006).
794 Nitrogen and Sulphur Deposition on regional and global scales: a multi-model evaluation. *Global*
795 *Biogeochemical Cycles*, **20**, GB4003.

796 Dezi, S., Medlyn, B. E., Tonon, G., & Magnani, F. (2010). The effect of nitrogen deposition on forest
797 carbon sequestration: a model-based analysis. *Global Change Biology*, **16**, 1470-1486.

798 Du, E., de Vries, W., Han, W., Liu, X. J., Yan, Z. B., & Jiang, Y. (2016). Imbalanced phosphorus and
799 nitrogen deposition in China's forests. *Atmospheric Chemistry and Physics*, **16**, 8571-8579.

800 Elser, J. J., Bracken, M. E. S., Cleland, E. E., Gruner, D. S., Harpole, W. S., Hillebrand, H., ..., Smith, J. E.
801 (2007). Global analysis of nitrogen and phosphorus limitation of primary producers in freshwater, marine
802 and terrestrial ecosystems. *Ecology Letters*, **10**, 1135-1142.

803 Field, C. B., Jackson, R. B., & Mooney, H. A. (1995). Stomatal responses to increased CO₂: implications
804 from the plant to the global scale. *Plant, Cell & Environment* **18**, 1214-1225.

805 Fernández-Martínez, M., Vicca, S., Janssens, I. A., Sardans, J., Luysaert, S., Campioli, M., ..., Penuelas, J.
806 (2014). Nutrient availability as the key regulator of global forest carbon balance. *Nature Climate Change*, **4**,
807 471-476.

808 Foley, J. A., DeFries, R., Asner, G. P., Barford, C., Bonan, G., & Carpen, S. R. (2005). Global
809 consequences of land use. *Science*, **309**, 570-574.

810 Gaige, E., Dail, D. B., Hollinger, D. Y., Davidson, E. A., Fernandez, I. J., Sievering, H., ..., Halteman W.
811 (2007). Changes in canopy processes following whole-forest canopy nitrogen fertilization of a mature
812 spruce-hemlock forest. *Ecosystems*, **10**, 1133-1147.

813 Galloway, J. N., Dentener, F. J., Capone, D. G., Boyer, E. W., Howarth, R. W., Seitzinger, S. P., ...,
814 Voosmarty, C. J. (2004). Nitrogen cycles: past, present, and future. *Biogeochemistry*, **70**, 153-226.

815 Giglio, L., Randerson, J. T., & van der Werf, G. R. (2013). Analysis of daily, monthly, and annual burned
816 area using the fourth- generation global fire emissions database (GFED4). *Journal of Geophysical*
817 *Research: Biogeosciences*, **118**, 317-328.

818 Gill, A. L., & Finzi, A. C. (2016). Belowground carbon flux links biogeochemical cycles and resource-use
819 efficiency at the global scale. *Ecology Letters*, **19**, 1419-1428.

820 Goll, D. S., Brovkin, V., Parida, B. R., Reick, C. H., Kattge, J., Reich, P. B., ..., Niinemets, U. (2012).
821 Nutrient limitation reduces land carbon uptake in simulations with a model of combined carbon, nitrogen
822 and phosphorus cycling. *Biogeosciences*, **9**, 3547-3569.

823 Goll, D. S. (2016) Coupled Cycling of Carbon, Nitrogen, and Phosphorus. In Soil Phosphorus (edited by
824 Lal Rattan Stewart, B. A.) Taylor & Francis Group, 6000 Broken Sound Parkway NW, Suite 300, Boca
825 Raton, FL 33487-2742 CRC Press.

826 Goodale, C. L., Lajtha, K., Nadelhoffer, K. J., Boyer, E. W., & Jaworski, N. A. (2002). Forest nitrogen
827 sinks in large eastern US watersheds: estimates from forest inventory and an ecosystem model. In *The*
828 *Nitrogen Cycle at Regional to Global Scales* (pp. 239-266). Springer Netherlands.

829 Goulden, M. L., McMillan, A. M. S., Winston, G. C., Rocha, A. V., Manies, K. L., Harden, J. W., &
830 Bond-Lamberty, B. P. (2011). Patterns of NPP, GPP, respiration, and NEP during boreal forest succession.
831 *Global Change Biology*, **17**, 855-871.

832 Graham, W. F., Duce, R. A. (1979). Atmospheric pathways of the phosphorus cycle. *Geochimica et*
833 *Cosmochimica Acta*, **43**, 1195-1208.

834 Granier, C., Bessagnet, B., Bond, T., D'AngiolaHugo, A., van der Gon, D., Frost, G. J., ..., Lioussé, C.
835 (2011). Evolution of anthropogenic and biomass burning emissions of air pollutants at global and regional
836 scales during the 1980-2010 period. *Climatic Change*, **109**, 163.

837 Gruber, N., & Galloway, J. N. (2008). An Earth-system perspective of the global nitrogen
838 cycle. *Nature*, **451**, 293-296.

839 Hansen, M. C., DeFries, R. S., Townshend, J. R., & Sohlberg, R. (2000). Global land cover classification at
840 1 km spatial resolution using a classification tree approach. *International Journal of Remote Sensing*, **21**,
841 1331-1364.

842 Hansen, M. C., Potapov, P. V., Moore, R., Hancher, M., Turubanova, S. A., Tyukavina, A., ..., Townshend,
843 J. R. G. (2013). High-resolution global maps of 21st-century forest cover change. *Science*, **342**, 850-853.

844 Hauglustaine, D. A., Balkanski, Y., & Schulz, M. (2014). A global model simulation of present and future
845 nitrate aerosols and their direct radiative forcing of climate. *Atmospheric Chemistry and Physics*, **14**,
846 11031-11063.

847 Hietz, P., Turner, B. L., Wanek, W., Richter, A., Nock, C. A., & Wright, S. J. (2011). Long-term change in
848 the nitrogen cycle of tropical forests. *Science*, **334**, 664-666.

849 Holland, E. A., Braswell, B. H., Lamarque, J. F., Townsend, A., Sulzman, J. Müller, J. F., ..., Roelofs, G. J.
850 (1997). Variations in the predicted spatial distribution of atmospheric nitrogen deposition and their impact
851 on carbon uptake by terrestrial ecosystems. *Journal of Geophysical Research: Atmospheres*, **102**,
852 15849-15866.

853 Houghton, R. A. (2003). Revised estimates of the annual net flux of carbon to the atmosphere from changes
854 in land use and land management 1850-2000. *Tellus B*, **55**, 378-390.

855 Hourdin, F., Musat, I., Bony, S., Braconnot, P., Codron, F., Dufresne, J. L., ..., Lott, F. (2006). The
856 LMDZ4 general circulation model: climate performance and sensitivity to parametrized physics with
857 emphasis on tropical convection. *Climate Dynamics*, **27**, 787-813.

858 Hungate, B. A., Stiling, P. D., Dijkstra, P., Johnson, D. W., Ketterer, M. E., Hymus, G. J., ..., Drake, B. G.
859 (2004). CO₂ elicits long-term decline in nitrogen fixation. *Science*, **304**, 1291-1291.

860 International Energy Agency (IEA). (2013). World Energy Statistics and Balances. Available at:
861 <http://www.oecd-ilibrary.org/statistics> (accessed August 22, 2013).

862 Iversen, C. M., McCormack, M. L., Powell, A. S., Blackwood, C. B., Freschet, G. T., Kattge, J., ..., Violle,
863 C. (2017). A global Fine-Root Ecology Database to address below-ground challenges in plant ecology. *New*
864 *Phytologist*, doi: 10.1111/nph.14486.

865 Johnson, A. H., Frizano, J., & Vann, D. R. (2003). Biogeochemical implications of labile phosphorus in
866 forest soils determined by the Hedley fractionation procedure. *Oecologia*, **135**, 487-499.

867 Keenan, T. F., Hollinger, D. Y., Bohrer, G., Dragoni, D., Munger, J. W., Schmid, H. P., & Richardson, A.
868 D. (2013). Increase in forest water-use efficiency as atmospheric carbon dioxide concentrations rise. *Nature*,
869 **499**, 324-327.

870 Klimont, Z., Smith, S. J., & Cofala, J. (2013). The last decade of global anthropogenic sulfur dioxide:
871 2000-2011 emissions. *Environmental Research Letter*, **8**, 014003.

872 Lamarque, J. F., Kiehl, J.T., Brasseur, G.P., Butler, T., Cameron-Smith, P., Collins, W.D., ..., Thornton, P.
873 (2005). Assessing future nitrogen deposition and carbon cycle feedback using a multimodel approach:
874 Analysis of nitrogen deposition. *Journal of Geophysical Research: Atmospheres*, **110**, D19303.

875 Lamarque, J. F., Bond, T. C., Eyring, V., Granier, C., Heil, A., Klimont, Z., ..., van Vuuren, D. P. (2010).
876 Historical (1850-2000) gridded anthropogenic and biomass burning emissions of reactive gases and
877 aerosols: methodology and application. *Atmospheric Chemistry and Physics*, **10**, 7017-7039.

878 Lamarque, J. F., Kyle, G. P., Meinshausen, M., Riahi, K., Smith, S. J., van Vuuren, D. P., ..., Vitt, F.
879 (2011). Global and regional evolution of short-lived radiatively-active gases and aerosols in the
880 Representative Concentration Pathways. *Climatic Change*, **109**, 191.

881 Lamarque, J. F., Dentener, F., McConnell, J., Ro, C. U., Shaw, M., Vet, R., ..., Nolan, M. (2013).
882 Multi-model mean nitrogen and sulfur deposition from the Atmospheric Chemistry and Climate Model
883 Intercomparison Project (ACCMIP): evaluation historical and projected changes. *Atmospheric Chemistry*
884 *and Physics*, **13**, 7997-8018.

885 Lathiere, J., Hauglustaine, D. A., Friend, A. D., Noblet-Ducoudré, N. D., Viovy, N., & Folberth, G. A.
886 (2006). Impact of climate variability and land use changes on global biogenic volatile organic compound
887 emissions. *Atmospheric Chemistry and Physics*, **6**, 2129-2146.

888 Le Quéré, C., Andrew, R. M., Canadell, J. G., Sitch, S., Korsbakken, J. I., Peters, G. P., ..., Zaehle, S.
889 (2016). Global carbon budget 2016. *Earth System Science Data*, **8**, 605.

890 LeBauer, D. S., & Treseder, K. K. (2008). Nitrogen limitation of net primary productivity in terrestrial
891 ecosystems is globally distributed. *Ecology*, **89**, 371-379.

892 Liu, L., & Greaver, T. L. (2009). A review of nitrogen enrichment effects on three biogenic GHGs: the CO₂
893 sink may be largely offset by stimulated N₂O and CH₄ emission. *Ecology Letters*, **12**, 1103-1117.

894 Lovett, G. M., & Lindberg, S. E. (1993). Atmospheric deposition and canopy interactions of nitrogen in
895 forests. *Canadian Journal of Forest Research*, **23**, 1603-1616.

896 Lü, X. T., Reed, S., Yu, Q., He, N. P., Wang, Z. W., Han, X. G. (2013). Convergent responses of nitrogen
897 and phosphorus resorption to nitrogen inputs in a semiarid grassland. *Global Change Biology*, **19**,
898 2775-2784.

899 Magnani, F., Mencuccini, M., Borghetti, M., Berbigier, P., Berninger, F., Delzon, S., ..., Grace, J. (2007).
900 The human footprint in the carbon cycle of temperate and boreal forests. *Nature*, **447**, 849-851.

901 Mahowald, N., Jickells, T. D., Baker, A. R., Artaxo, P., Benitez-Nelson, C. R., Bergametti, G., ..., Tsukuda,
902 S. (2008). Global distribution of atmospheric phosphorus sources, concentrations and deposition rates, and
903 anthropogenic impacts. *Global Biogeochemical Cycles*, **22**, GB4026.

904 Mahowald, N. (2011). Aerosol indirect effect on biogeochemical cycles and climate. *Science*, **334**,

905 794-796.

906 Marklein, A. R., & Houlton, B. Z. (2012). Nitrogen inputs accelerate phosphorus cycling rates across a
907 wide variety of terrestrial ecosystems. *New Phytologist*, **193**, 696-704.

908 Matthews, H. D. (2007). Implications of CO₂ fertilization for future climate change in a coupled
909 climate-carbon model. *Global Change Biology*, **13**, 1068-1078.

910 Nadelhoffer KJ, Emmett BA, Gundersen P, Kjønaas, O. J., Koopmans, C. J., Schleppi, P., ..., Wright, R. F.
911 (1999). Nitrogen deposition makes a minor contribution to carbon sequestration in temperate
912 forests. *Nature*, **398**, 145-148.

913 Nair, R. K., Perks, M. P., Weatherall, A., Baggs, E. M., & Mencuccini, M. (2016). Does canopy nitrogen
914 uptake enhance carbon sequestration by trees? *Global change biology*, **22**, 875-888.

915 Norby, R. J., Warren, J. M., Iversen, C. M., Medlyn, B. E., & McMurtrie, R. E. (2010). CO₂ enhancement
916 of forest productivity constrained by limited nitrogen availability. *Proceedings of the National Academy of*
917 *Sciences*, **107**, 19368-19373.

918 Okin, G. S., Mahowald, N., Chadwick, O. A., & Artaxo, P. (2004). Impact of desert dust on the
919 biogeochemistry of phosphorus in terrestrial ecosystems. *Global Biogeochemical Cycles*, **18**, GB2005.

920 Paulot, F., Jacob, D. J., & Henze, D. K. (2013). Sources and processes contributing to nitrogen deposition:
921 An adjoint model analysis applied to biodiversity hotspots worldwide. *Environmental Science &*
922 *Technology*, **47**, 3226-3233.

923 Paulot, F., Jacob, D. J., Johnson, M. T., Bell, T. G., Baker, A. R., Keene, W. C., ..., Stock, C. A. (2015).
924 Global oceanic emission of ammonia: Constraints from seawater and atmospheric observations. *Global*
925 *Biogeochemical Cycles*, **29**, 1165-1178.

926 Peng, S., Ciais, P., Maignan, F., Li, W., Chang, J. F., Wang, T., & Yue, C. (2017). Sensitivity of land-use
927 change emission estimates to historical land-use and land-cover mapping. *Global Biogeochemical Cycles*,
928 **31**, doi:10.1002/2015GB005360.

929 Peñuelas, J., Sardans, J., Rivas- Ubach, A., & Janssens, I. A. (2012). The human- induced imbalance
930 between C, N and P in Earth's life system. *Global Change Biology*, **18**, 3-6.

931 Penuelas, J., Poulter, B., Sardans, J., Ciais, P., van der Velde, M., Bopp, L., ..., Janssens, I. A. (2013).
932 Human-induced nitrogen–phosphorus imbalances alter natural and managed ecosystems across the
933 globe. *Nature Communications*, **4**, 2934.

934 Phillips, O. L., Aragão, L. E. O. C., Lewis, S. L., Fisher, J. B., Lloyd, J., López-González, G., ...,
935 Torres-Lezama, A. (2009). Drought sensitivity of the Amazon rainforest. *Science*, **323**, 1344-1347.

936 Phoenix, G. K., Hicks, W. K., Cinderby, S., Kuylenstierna, J. C. I., Stock, W. D., Dentener, F. J., ...,
937 Ineson, P. (2006). Atmospheric nitrogen deposition in world biodiversity hotspots: the need for a greater
938 global perspective in assessing N deposition impacts. *Global Change Biology*, **12**, 470-476.

939 Piao, S., Ciais, P., Friedlingstein, P., Peylin, P., Reichstein, M., Luysaert, S., ..., Vesala, T. (2008). Net
940 carbon dioxide losses of northern ecosystems in response to autumn warming. *Nature*, **451**, 49-52.

941 Reay, D. S., Dentener, F., Smith, P., Grace, J., & Feely, R. A. (2008). Global nitrogen deposition and
942 carbon sinks. *Nature Geoscience*, **1**, 430-437.

943 Reed, S. C., Yang, X., & Thornton, P. E. (2015). Incorporating phosphorus cycling into global modeling
944 efforts: a worthwhile, tractable endeavor. *New Phytologist*, **208**, 324-329.

945 Reich, P. B., Hobbie, S. E., Lee, T., Ellsworth, D. S., West, J. B., Tilman, D., ..., Trost, J. (2006). Nitrogen
946 limitation constrains sustainability of ecosystem response to CO₂. *Nature*, **440**, 922-925.

947 Riahi, K., Grübler, A., & Nakicenovic, N. (2007). Scenarios of long-term socio-economic and
948 environmental development under climate stabilization. *Technological Forecasting and Social Change*, **74**,
949 887-935.

950 Rowe, E. C., Smart, S. M., Kennedy, V. H., Emmett, B. A., & Evans, C. D. (2008). Nitrogen deposition
951 increases the acquisition of phosphorus and potassium by heather *Calluna vulgaris*. *Environmental*
952 *Pollution*, **155**, 201-207.

953 Sardans, J., & Peñuelas, J. (2013). Tree growth changes with climate and forest type are associated with
954 relative allocation of nutrients, especially phosphorus, to leaves and wood. *Global Ecology and*
955 *Biogeography*, **22**, 494-507.

956 Sardans, J., & Peñuelas, J. (2015) Potassium: a neglected nutrient in global change. *Global Ecology and*
957 *Biogeography*, **24**, 261-275.

958 Sattari, S. Z., Bouwman, A. F., Giller, K. E., & van Ittersum, M. K. (2012). Residual soil phosphorus as the
959 missing piece in the global phosphorus crisis puzzle. *Proceedings of the National Academy of Sciences*, **109**,
960 6348-6353.

961 Schlesinger, W. H. (2009). On the fate of anthropogenic nitrogen. *Proceedings of the National Academy of*
962 *Sciences*, **106**, 203-208.

963 Sievering, H., Tomaszewski, T., & Torizzo, J. (2007). Canopy uptake of atmospheric N deposition at a
964 conifer forest: part I- canopy N budget, photosynthetic efficiency and net ecosystem exchange. *Tellus B*, **59**,
965 483-492.

966 Sparks, J. P. (2009). Ecological ramifications of the direct foliar uptake of nitrogen. *Oecologia*, **159**, 1-13.

967 Templer, P. H., Mack, M. C., Chapin III, F. S., Christenson, L. M., Compton, J. E., Crook, H. D., ..., Zak,
968 D. R. (2012). Sinks for nitrogen inputs in terrestrial ecosystems: a meta- analysis of 15N tracer field
969 studies. *Ecology*, **93**, 1816-1829.

970 Thomas, R. Q., Canham, C. D., Weathers, K. C., & Goodale, C. L. (2010). Increased tree carbon storage in
971 response to nitrogen deposition in the US. *Nature Geoscience*, **3**, 13-17.

972 Thornton, P. E., Doney, S. C., Lindsay, K., Moore, J. K., Mahowald, N., Randerson, J. T., ..., Lee, Y. H.
973 (2009). Carbon-nitrogen interactions regulate climate-carbon cycle feedbacks: results from an
974 atmosphere-ocean general circulation model. *Biogeosciences*, **6**, 2099-2120.

975 Tipping, E., Benham, S., Boyle, J. F., Crow, P., Davies, J., Fischer, U., ..., Toberman, H. (2014).
976 Atmospheric deposition of phosphorus to land and freshwater. *Environmental Science: Processes &*
977 *Impacts*, **16**, 1608-1617.

978 van der Werf, G. R., Randerson, J. T., Collatz, G. J., Giglio, L., Kasibhatla, P. S., Arellano Jr, A. F., ...,
979 Kasischke, E. S. (2004). Continental-scale partitioning of fire emissions during the 1997 to 2001 El
980 Nino/La Nina period. *Science*, **303**, 73-76.

981 Vet, R., Artz, R. S., Carou, S., Shaw, M., Ro, C. U., Aas, W., ..., Reid, N. W. (2014). A global assessment
982 of precipitation chemistry and deposition of sulfur, nitrogen, sea salt, base cations, organic acids, acidity
983 and pH, and phosphorus. *Atmospheric Environment*, **93**, 3-100.

984 Vitousek, P. M. (1984). Litterfall, nutrient cycling, and nutrient limitation in tropical forests. *Ecology*, **65**,
985 285-298.

986 Vitousek, P. M., Porder, S., Houlton, B. Z., & Chadwick, O. A. (2010). Terrestrial phosphorus limitation:
987 mechanisms, implications, and nitrogen–phosphorus interactions. *Ecological Applications*, **20**, 5-15.

988 Walker, T. W., & Syers, J. K. (1976). The fate of phosphorus during pedogenesis. *Geoderma*, **15**, 1-19.

989 Wang, Y. P., Law, R. M., & Pak, B. (2010). A global model of carbon, nitrogen and phosphorus cycles for
990 the terrestrial biosphere. *Biogeosciences*, **7**, 2261-2282.

991 Wang, R., Balkanski, Y., Boucher, O., Ciais, P., Peñuelas, J., & Tao, S. (2015a). Significant contribution of
992 combustion-related emissions to the atmospheric phosphorus budget. *Nature Geoscience*, **8**, 48-54.

993 Wang, R., Balkanski, Y., Bopp, L., Aumont, O., Boucher, O., Ciais, P., ..., Tao, S. (2015b). Influence of
994 anthropogenic aerosol deposition on the relationship between oceanic productivity and
995 warming. *Geophysical Research Letters*, **42**, 10745-10754.

996 Westerling, A. L., Hidalgo, H. G., Cayan, D. R., & Swetnam, T. W. (2006). Warming and earlier spring
997 increase western US forest wildfire activity. *Science*, **313**, 940-943.

998 Wieder, W. R., Cleveland, C. C., Smith, W. K., & Todd-Brown, K. (2015). Future productivity and carbon
999 storage limited by terrestrial nutrient availability. *Nature Geoscience*, **8**, 441-444.

1000 Xu, X., Thornton, P. E., & Post, W. M. (2013). A global analysis of soil microbial biomass carbon,
1001 nitrogen and phosphorus in terrestrial ecosystems. *Global Ecology and Biogeography*, **22**, 737-749.

1002 Yang, X., Post, W. M., Thornton, P. E., & Jain, A. (2013). The distribution of soil phosphorus for global
1003 biogeochemical modeling. *Biogeosciences*, **10**, 2525.

1004 Yang, X., Thornton, P. E., Ricciuto, D. M., & Post, W. M. (2014). The role of phosphorus dynamics in
1005 tropical forests. *Biogeosciences*, **11**, 1667.

1006 Zaehle, S., Friedlingstein, P., & Friend, A. D. (2010). Terrestrial nitrogen feedbacks may accelerate future
1007 climate change. *Geophysical Research Letters*, **37**, L01401.

1008 Zaehle, S., Medlyn, B. E., De Kauwe, M. G., Walker, A. P., Dietze, M. C., Hickler, T., ..., Norby, R. J.
1009 (2014). Evaluation of 11 terrestrial carbon-nitrogen cycle models against observations from two temperate
1010 Free- Air CO₂ Enrichment studies. *New Phytologist*, **202**, 803-822.

1011 Zhu, Z., Piao, S., Myneni, R. B., Huang, M. T., Zeng, Z. Z., Canadell, J. G., ..., Zeng, N. (2016). Greening
1012 of the Earth and its drivers. *Nature Climate Change*, **6**, 791-795.